Progress in Organic Coatings 188 (2024) 108262

Contents lists available at ScienceDirect

Progress in Organic Coatings

journal homepage: www.elsevier.com/locate/porgcoat

Exploring polyamide 11 as a novel renewable resource-based filler in wood paint: Investigating aesthetic aspects and durability impact of the composite coating

Massimo Calovi *, Stefano Rossi

Department of Industrial Engineering, University of Trento, Via Sommarive 9, 38123 Trento, Italy

ARTICLE INFO

Keywords:
Polyamide 11
Bio-based additive
Wood paint
Protective coating
Abrasion resistance

ABSTRACT

The aim of this study is to assess the impact of different quantities of polyamide 11 powder on the visual appeal, durability, and multi-functionality of a water-based wood paint. To investigate the effect of this bio-based additive on the overall appearance of the coatings, measurements for color, gloss, and surface roughness were conducted. Additionally, various tests were performed to quantify the influence of these environmentally friendly additives on the mechanical properties of the coatings, including hardness, surface friction coefficient, and resistance to abrasion. Moreover, the effect of varying amounts of polyamide 11 powder on the coating's barrier capabilities was evaluated through liquid resistance tests, contact angle measurements, and water uptake assessment. Finally, the influence of the bio-based additive on the layers' durability was evaluated by subjecting them to exposure in a xenon arc light chamber. The degradation of the samples was monitored through colorimetric inspections to assess any changes or deterioration. In summary, this study underscores the significant impact of varying the quantity of polyamide 11 powder, showcasing its ability to not only introduce distinct texture to the paint but also significantly enhance the mechanical properties of the composite layer. Importantly, these improvements are achieved without compromising the barrier properties and durability of the acrylic matrix coating.

1. Introduction

The coatings industry has long been integral to the economies of numerous nations [1]. Preserving components and ensuring their durability holds considerable economic significance [2], prompting continuous innovative research into improving protective layer properties to extend the lifespan of industrial parts [3]. Presently, there's an implicit anticipation for coatings to offer substantial protection to the underlying surface. Additionally, contemporary developments emphasize aesthetic aspects such as color [4] and specific texture [5] of these protective coatings. Consequently, coatings are expected not only to provide protection but also to offer visual appeal [6].

Nevertheless, a prevailing and swiftly expanding movement contends that a solitary coating should not solely focus on being protective and visually attractive; it should also possess supplementary capabilities [6]. These capabilities might include robust resistance to abrasion [7], responsiveness to external factors like temperature [8] or light [9], demonstration of antibacterial properties [10], and integration of additives facilitating thermal and electrical conductivity [11,12]. These functionalities find significant utility in advanced industrial sectors reliant on high technology [13,14]. While these features are often linked with metallic [15] and ceramic coatings [16], they are also notably associated with organic coatings and paints [17].

Paints stand as one of the most extensively employed coatings worldwide, utilized on surfaces encompassing both metallic and wooden substrates. Particularly, wood has consistently ranked among the most utilized materials [18] across diverse industrial domains, prized for its ease of manipulation [19], distinct chemical [20], and physical [21] characteristics, as well as its widespread availability. Furthermore, in an era increasingly focused on environmental preservation, wood garners favor as a renewable and biodegradable resource with no CO_2 footprint.

Nonetheless, wood demands vigilant measures, such as the application of protective coatings [22,23], to mitigate the physical-chemical deterioration of its lignocellulosic elements instigated by factors like solar radiation [24], moisture infiltration into its structure [25], potential mechanical harm [26], chemical-induced damage [27], and

* Corresponding author.
E-mail address: massimo.calovi@unitn.it (M. Calovi).

https://doi.org/10.1016/j.porgcoat.2024.108262
Received 30 November 2023; Received in revised form 29 December 2023; Accepted 15 January 2024
Available online 20 January 2024

safeguarding against detrimental microorganisms like fungi [28]. In this context, studies have concentrated on enhancing the protective attributes of wood coatings, often by integrating specific functional additives [29]. For instance, metallic and ceramic nanopowders have exhibited an effective shielding capacity against UV radiation [30,31] and contributed significantly to augmenting wood's hardness and stiffness [32,33], while substantially reducing water absorption within the coating [34]. Furthermore, metallic nanomaterials have been utilized to confer efficient antibacterial and antifungal functions to the coating [35,36].

Moreover, the wood coating industry is currently directing its attention towards two significant and pivotal focal points: eco-friendly materials and the principles of a circular economy. As the sector progressively seeks environmentally sustainable and versatile alternatives to traditional synthetic additives [37], which often overlook environmental sustainability in their production [38], scientific inquiry is exploring the incorporation of organic supplements in coatings [39]. To achieve this objective, researchers have recently investigated the effects of incorporating various elements into wood coatings. These include substances such as bio-based oils [40,41], cellulose derivatives [42,43], colorants sourced from wood byproducts [44], microbial-based pigmentation [45], and dyes extracted from fungi [46], spices [47] and microalgae [48–50].

From this perspective, polyamide 11 powders emerge as a compelling bio-derived resource, offering potential as a versatile and environmentally friendly additive for wood paints. Arkema (Colombes, France) manufactures this material under the commercial name Rilsan®, crafting micrometric powder from 100 % renewable sources like castor oil. Rilsan® polyamide 11 (PA11) has gained worldwide recognition as the go-to choice for flexible polyamide resins renowned for their exceptional impact resistance, durability, and chemical resilience. Its unique crystalline structure sets this polymer apart from its petroleum-derived counterparts. The resin used in producing PA11 powders is notably lightweight while maintaining long-term durability and strength [51]. Additionally, this pioneering material showcases commendable dimensional stability and provides impressive impact and abrasion resistance characteristics [52,53]. These attributes distinguish PA11 as an exceptionally compelling form of polyamide for use in organic coatings and paints. However, despite these notable qualities, the multifunctional potential of PA11 powders as a paint filler has yet to be explored in existing literature.

Therefore, considering the interesting features and green aspects of the PA11 powders, this research aims to investigate the diverse impact of incorporating this bio-based additive on the functionality of a water-based wood paint. The study not only evaluates the aesthetic enhancements and multifunctional characteristics introduced by the PA11 powder but also examines the impact of different amounts of filler on the durability of the polymer coating.

2. Materials and methods

2.1. Materials

The polyamide 11 (PA11) powder, called Rilsan® D60 NAT, was supplied by Grolman Group (Merate, Italy) and used as received. The product appears as a white powder, consisting of granules that typically measure between 43 and 55 μm in size. The polymer boasts a melting point of 186 °C and a density of 0.38 g/cm^3. Poplar wood panels sized at 150 × 150 × 2 mm^3 were obtained from Cimadom Legnami (Lavis, TN, Italy). The panels possess a density ranging between 0.40 and 0.42 g/cm^3 and a moisture content falling within the 6 to 9 % range. Poplar plywood was selected as the substrate for applying the paint due to its esteemed reputation for exceptional quality compared to other panel materials [54]. Its notably smooth surface renders it ideal for painting, laminating, or veneering purposes [55]. Moreover, its ease of machining, particularly its reputation for effortless cutting, sanding, or screwing, makes it a preferred choice for preparing diverse samples intended for various characterization tests. The water-based acrylic paint known as TECH20 was purchased from ICA Group (Civitanova Marche, AN, Italy). This paint formulation is created using materials sourced from sustainable and renewable sources. The product has a specific weight of 1.01–1.18 g/ml and a viscosity of 50–60 s Ford Cup 5. Sodium chloride (with a minimum purity of 99.0 %) and ethanol (with a purity of 99.8 %) were acquired from Sigma-Aldrich (St. Louis, MO, USA), and used in their original state. To conduct tests for liquid resistance, the following items were acquired: Suma Bac D10 Cleaner and Sanitizer, a commercial detergent disinfectant from Diversey (Fort Mill, SC, USA), containing benzalkonium chloride within the range of 3.0–10.0 wt%, and Catafor 502XC cataphoretic red ink manufactured by Arsonsisi (Milan, MI, Italy).

2.2. Samples production

To achieve even paint coverage, the wooden base underwent a pretreatment process involving rubbing it with 320 grit paper until achieving a smooth surface. Subsequently, the paint was applied using a spray method following the guidelines provided by the supplier. The application involved utilizing a pressure of 3 bar and a material rate of 100 g/m^2. Four distinct sets of samples were generated, as outlined in Table 1, by adjusting the paint composition through the addition of varying amounts of PA11 powder. To ensure a consistent distribution of the additive within the paint, each solution underwent mechanical mixing for 30 min before being applied to the wooden base. Due to the lower density of the filler compared to the paint, initially, PA11 powders have a tendency to float within the paint. Nevertheless, the mixing treatment facilitates a uniform dispersion of the filler in the solution, resulting in an absence of sinking or floating phenomena of the PA11 powder. Following application, the paint coating was allowed to air cure for 4 h at room temperature. This deposition and curing process was repeated twice for each sample type to achieve a consistent and uniform coating thickness. The evaluation of the bio-based additive's impact involved comparing the performance of these samples against sample P0.0, which serves as the reference, as it was produced using the standard paint without any PA11 addition.

2.3. Characterization

2.3.1. PA11 characterization

The bio-based filler underwent characterization on both a morphological and chemical level. Morphological observations were conducted using the low vacuum scanning electron microscope SEM JEOL IT 300 (JEOL, Akishima, Tokyo, Japan). Chemical analysis was performed through FTIR infrared spectroscopy using a Varian 4100 FTIR Excalibur spectrometer (Varian, Santa Clara, CA, USA).

2.3.2. Appearance and morphological features of the coatings

SEM was utilized to examine both the surface and cross-section of the coatings. This assessment aimed to determine if the presence of PA11 powders had any impact on the structural morphology of the layers. The impact of the filler on both the surface characteristics and appearance was assessed through measurements of surface roughness, color, and gloss of the coatings. Surface roughness was gauged using the MarSurf PS1 mobile surface roughness measurement instrument from Carl Mahr Holding (Gottingen, Germany). Colorimetric analysis was conducted

Table 1
Samples nomenclature.

Samples nomenclature	Amount of PA11 powder (wt%)
P0.0	/
P0.1	0.1
P1.0	1.0
P10.0	10.0

using a Konica Minolta CM-2600d spectrophotometer (Konica Minolta, Tokyo, Japan) employing a D65/10° illuminant/observer configuration in SCI mode. Gloss was evaluated using an Erichsen 503 instrument from Erichsen Cofomegra Instruments (Milan, Italy), following the ASTM D523/14 standard [56]. 25 roughness, color and gloss assessments were performed on 5 samples per series (with 5 measurements per sample).

2.3.3. Mechanical properties of the coatings

The impact of the bio-based additive content on the mechanical properties of the polymer matrix was assessed through several tests. The hardness of the coatings was examined using the Buchholz hardness indentation test, following the ISO 2815 standard [57]. An Elcometer 3095 Buchholz Hardness Tester (Elcometer, Manchester, UK) was utilized for this test, featuring a beveled disc indentation tool with a sharp edge inserted into a stainless steel block. A consistent testing force of 500 g was applied for 30 s on the coating surface. The extent of the impression made by the standardized instrument provided an indication of the coatings' hardness. 15 measurements were performed on 5 samples per series (with 3 measurements per sample).

The static coefficient of friction (COF) for the various coatings was determined using an experimental setup similar to those used in prior studies [58,59]. A weight of 0.5 kg was applied to the samples, and they were pulled using a dynamometer at a speed of 0.1 cm/s. The instrument measured the force required to move the sample, allowing for the calculation of the COF. The test results represent the average of five measurements conducted for each series of samples (100 × 70 × 2 mm^3).

The anti-abrasive properties of PA11 powders were investigated using two specific tests. The more aggressive Taber test was conducted on 5 samples per series (100 × 100 × 2 mm^3) utilizing a TABER 5135 Rotary Platform Abrasion Tester (Taber Industries, North Tonawanda, NY, USA) in accordance with the guidelines outlined in the ASTM D4060–10 standard [60]. This test involved employing two CS17 abrasion wheels with an associated total weight of 500 g, subjecting the samples to a total of 3000 Taber cycles while monitoring the extent of mass loss. After the test, the abrasion profile was evaluated using a Waveline W600 roughness meter (OGP HOMMEL, Desio, MB, Italy) to analyze how the filler contributed to reducing abrasive wear. Furthermore, SEM was utilized to observe the morphology of the samples, providing insights into how the two additives responded to the abrasive phenomenon. The SEM was used as the final step to observe the sample morphology, offering insights into how the additive reacted or behaved in response to the abrasive phenomenon.

The scrub test, less aggressive compared to the previous one, aimed to gather specific information about the role and behavior of the filler when exposed to abrasive stresses. Conducted on 5 samples per series (150 × 80 × 2 mm^3) using an Elcometer 1720 Abrasion and Washability Tester (Elcometer, Manchester, UK), the test followed the ISO 11998 standard [61], employing the standardized sponge Tool 5 with a weight of 232 g. It's noteworthy that, unlike the standard procedure, this test was carried out in a dry mode without using a cleaning solution. This adjustment was made to prevent the test solution from penetrating the polymeric matrix and wood, which could potentially influence the outcomes. Mass loss from the coatings was monitored after every 250 cycles (operated at a frequency of 37 cycles per min) until reaching 1000 cycles. Similar to previous tests, SEM observations were employed to evaluate the impact of the test on the samples' morphology, focusing on understanding the role of the bio-based additive in counteracting the abrasive process. Additionally, the effects of the abrasive test on the coating's aesthetic properties were assessed by conducting analyses of gloss and roughness.

2.3.4. Barrier properties of the coatings

The impact of varying amounts of the bio-based additive on the acrylic matrix's barrier properties was explored using chemical resistance tests following the GB/T 1733–93 standard [62]. This involved immersing circular filter paper (radius = 2 cm) in four different solutions: 15 % sodium chloride, 70 % ethanol, detergent, and red ink. Each saturated filter paper was placed on the coating surface under a glass sheet for 24 h. Afterward, any remaining liquid on the coating surface was absorbed, and colorimetric analysis was employed to detect imprints and color changes. 5 samples (60 × 60 × 2 mm^3) per series were subjected to the test.

Additionally, a liquid water absorption test, as per the EN 927-05 standard [63], was conducted to evaluate the coatings' water permeability. Poplar wood panels measuring 60 × 60 × 2 mm^3 had five uncoated surfaces sealed hermetically with silicone to prevent water absorption by the wood substrate. The samples, conditioned at 65 % relative humidity and 20 °C, were then placed in water for specific durations (6, 24, 48, 72, and 96 h), and the moisture absorption (expressed in grams per square meter - g/m^2) was calculated by measuring the change in mass before and after each duration. 5 samples per series were subjected to the water absorption test.

Moreover, contact angle measurements, conducted in adherence to the ASTM D7334-08 standard [64], were aimed at assessing the influence of PA11 powders on the coating's wettability. Utilizing a Nikon 60 mm lens with an aperture of f/2.8 (Nikon Instruments Europe, Amstelveen, the Netherlands), macro images were captured. The contact angle measurement was executed using the NIS-Elements Microscope Imaging software (Windows Version 4.30.01). Demineralized water droplets (5 μl), generated via a syringe and dispersed from approximately 2 cm away, were the focus. 60 s after deposition on the coating, the drop was photographed, and the wetting angle was calculated using the imaging software. To ensure statistical validity, each sample underwent 10 measurements, enabling a thorough analysis of the surface wettability properties.

2.3.5. Durability of the coatings

Lastly, to evaluate the impact of the additive on the coating's durability in outdoor settings, accelerated degradation tests were conducted following the ASTM G155-05 standard [65]. The samples underwent exposure in a Xenon Arc Light Apparatus Q-SUN Xe-1 Xenon Test Chamber from Q-Lab Corporation (Westlake, OH, USA). This exposure lasted 300 h under conditions simulating solar radiation (60 W/m^2 at 50 °C). The resistance of the coatings against degradation caused by this simulated exposure was assessed. 5 samples (80 × 50 × 2 mm^3) per series were subjected to the test. The physical decay of the composite layers was measured using colorimetric analyses and gloss measurements. The test concluded at 300 h of exposure since all the samples exhibited consistent chromatic and gloss stability at that point.

3. Results and discussion

3.1. Filler and coatings morphology

Fig. 1a displays the morphological appearance of PA11 powders as observed with SEM. The image includes an enlargement highlighting the aspect of the granules, varying in size but generally averaging around 50 μm, as specified by the manufacturer. In addition, these powders exhibit an irregular morphology with a notably rough surface, as highlighted in previous studies [66]. Fig. 1b, instead, displays the FTIR spectrum of the granules, attributable to the typical output of PA11 [67,68]. The peak at 3299 cm^{-1} can be attributed to the N—H stretching [67], while the two signals at 2917 and 2849 cm^{-1} are associated to the CH_2 asymmetric and symmetric stretching, respectively [68]. The intense peak at 1633 cm^{-1} corresponds to the C═O stretching (amide I) [69], and the band at 1535 cm^{-1} refers to the C—N stretching and C═O in plane bending. The signal at 1467 cm^{-1} is attributed to the C═O and N-vicinal CH_2 bending [67], while the peak at 1222 cm^{-1} is associated with the C—N stretching [68]. Finally, the band at 676 cm^{-1} refers to the CONH out-of-plane deformation (amide V), typical of PA11 [69].

PA11 powder was therefore added to the acrylic paint at various

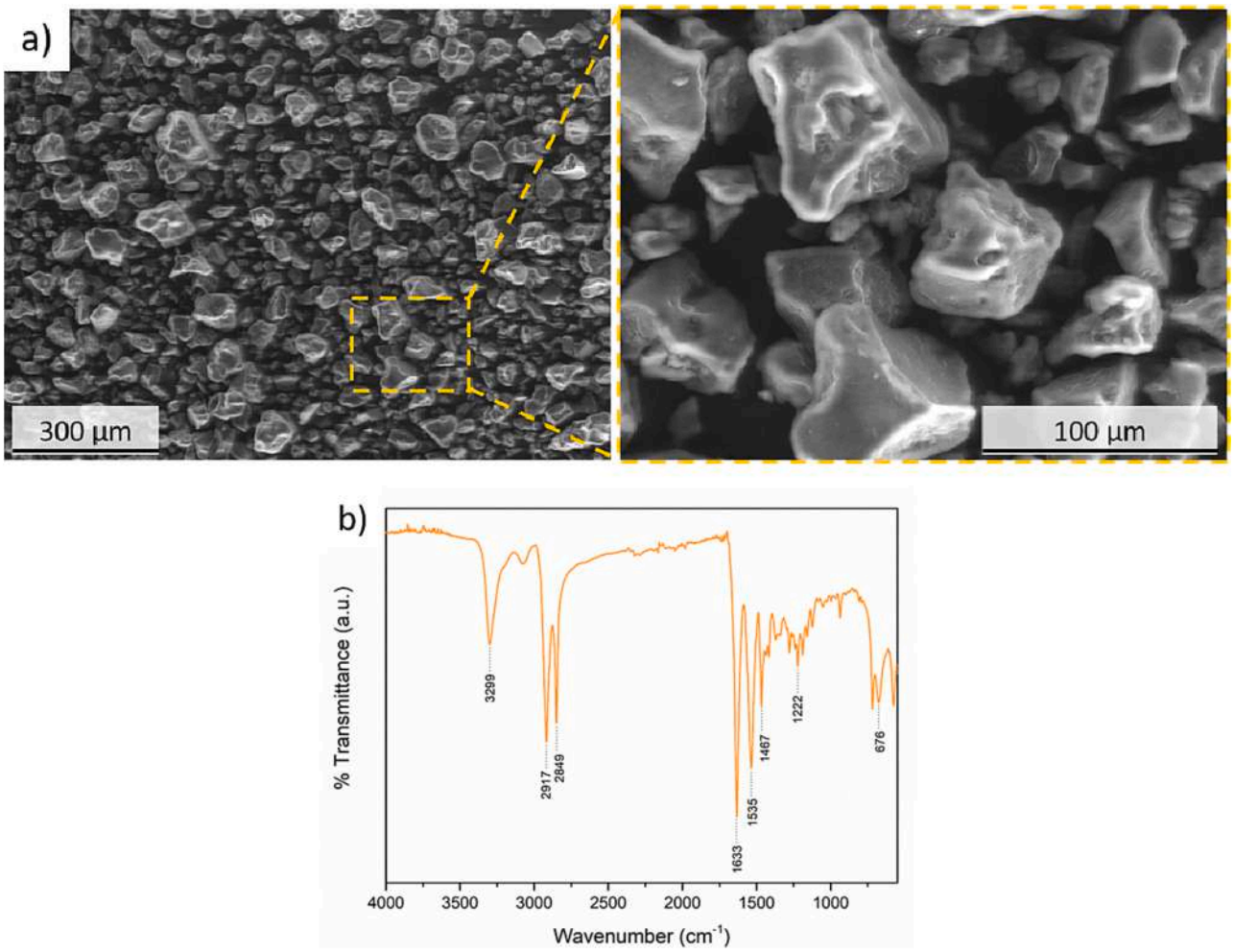

Fig. 1. a) SEM micrographs of the PA11 powder and b) its FTIR spectrum.

concentrations, to produce the four series of samples described in Table 1. The FTIR spectra of the coating series are shown in Fig. S1 of the Supplementary materials. Fig. 2 comprises several images captured via SEM: on the left, the surface of the samples is shown in a top-view, while on the right, the coatings' cross-sections are displayed, focusing particularly on the internal morphological structure of the composite layers. Fig. 2a refers to the P0.0 sample, taken as a reference as it does not contain PA11 powder. The layer appears compact, devoid of significant defects, and homogeneous, with a thickness of approximately 140 µm. A thickness of this scale is well-suited to contain and accommodate fillers that share similar dimensions to PA11 powders. Sample P0.1 appears very similar (Fig. 2b) to the reference, with a coating showing limited defects and consistent thickness. This is due to the low concentration of the bio-based additive within, insufficient to influence the morphology of the final product. The initial impact of the PA11 filler becomes evident in sample P1.0 (Fig. 2c), highlighting two specific phenomena. Firstly, the coating surface is no longer homogeneous and flat; instead, it contains PA11 granules that increase the roughness of the layer. Simultaneously, the internal structure of the coating is necessarily altered by the presence of the additive: within the layer's cross-section, it's possible to observe some cavities previously occupied by PA11 granules, removed during the brittle fracture process in liquid nitrogen that the sample underwent. The intensity of these two phenomena is heightened with the increase in filler quantity, as highlighted in sample P10.0 (Fig. 2d). The coating's surface is notably rough, with several granules (individual and agglomerated) protruding from the bulk of the layer. The cross-section of the coating exhibits a more significant presence of the filler, with various cavities previously occupied by the granules. However, some PA11 powders are still well adhered to the coating, demonstrating an overall good compatibility between the filler and the polymeric matrix of the paint. As a result, the substantial presence of the bio-based filler has a significant impact on the internal structure of the coating, altering several surface features as well.

In this sense, for example, the roughness of the layer is greatly influenced by the quantity of PA11, as already highlighted by the top-view images in Fig. 2. Table 2 displays the evolution of the samples' roughness [Ra] with the increase in PA11 content. The output of the table represents an average of 25 assessments performed on 5 samples per series (with 5 measurements per sample). These evaluations were conducted in both parallel (//Ra) and perpendicular (⊥Ra) orientations concerning the fibers of the wooden substrate. Due to the acrylic paint conforming to the wooden substrate's morphology, the perpendicular roughness of the reference sample P0.0 notably exceeds the roughness observed parallel to the fibers. These values are not substantially influenced in sample P0.1 but begin to increase when the quantity of PA11 within the coating becomes more significant, as seen in sample P1.0, where the values of //Ra start approaching values similar to ⊥Ra, representing an almost uniform level of roughness in both directions, no longer exhibiting morphological anisotropy. Lastly, sample P10.0 displays significantly higher levels of roughness in both directions, confirming the high presence of the filler near the surface of the coating. These values align with the specific morphologies of accumulations observed in top-view in Fig. 2d, indicative of the substantial content of the bio-based additive.

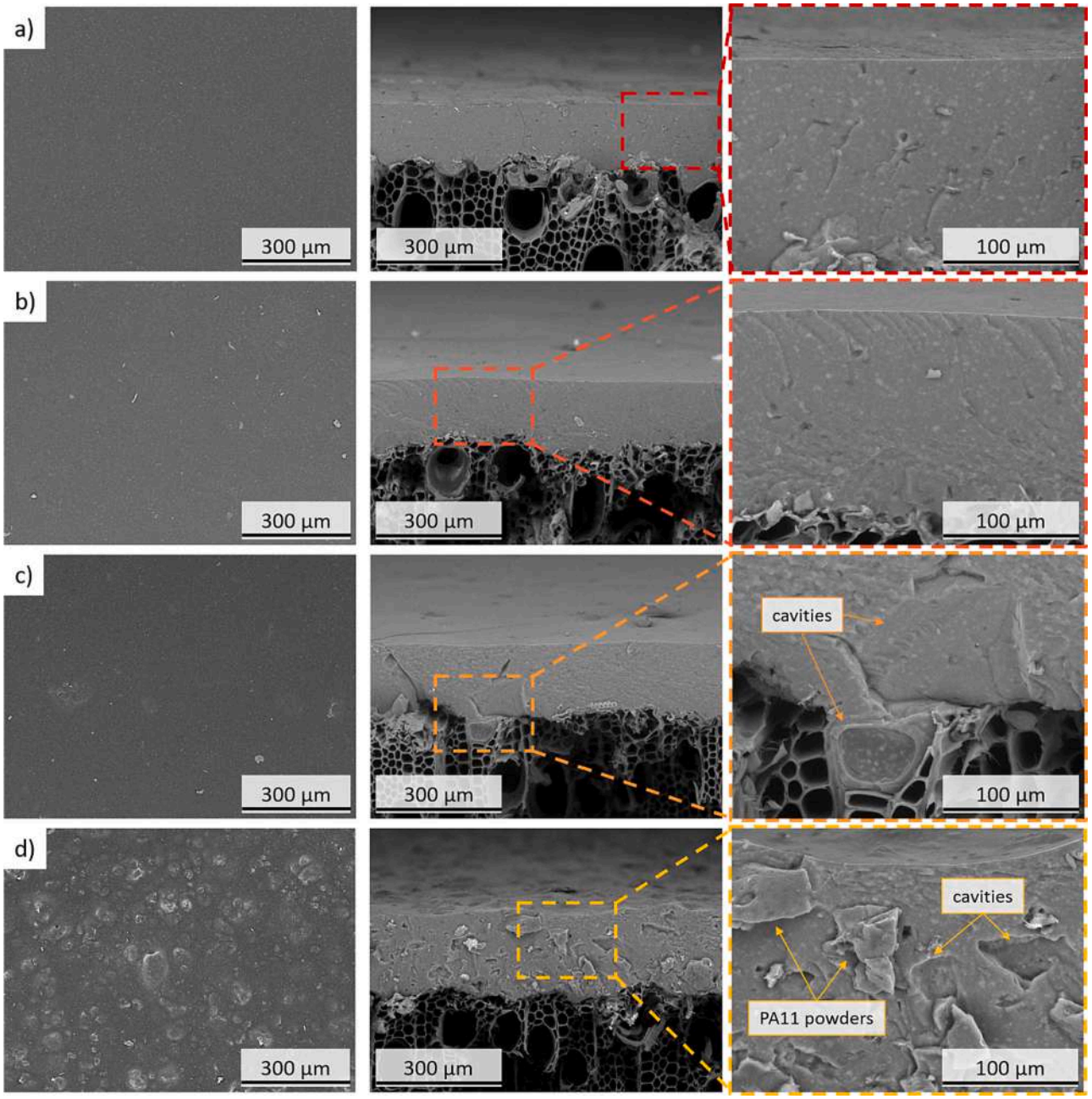

Fig. 2. SEM micrographs of the top-view (on the left) and cross-section (on the right) of a) sample P0.0, b) sample P0.1, c) sample P1.0 and d) sample P10.0.

Table 2
Coatings surface roughness.

Sample	Parallel roughness//Ra [µm]	Perpendicular roughness ⊥Ra [µm]
P0.0	0.35 + 0.06	1.12 + 0.28
P0.1	0.40 + 0.09	1.26 + 0.25
P1.0	1.11 + 0.38	1.28 + 0.33
P10.0	3.21 + 0.36	3.38 + 0.53

Given the relatively larger size of the fillers compared to the layer thickness, discussing the uniform distribution of PA11 powders based solely on section observations is challenging. However, the consistent color of the paint without any noticeable sinking or floating of particles, coupled with the consistent appearance of the coatings even through top-view observations, strongly implies a homogeneous distribution of the filler across the various coatings. Naturally, a substantial increase in the quantity of added PA11, as seen in sample P10.0, leads to inevitable agglomeration phenomena, causing the described increase in roughness.

These purely morphological aspects consequently impact the aesthetic characteristics of the coatings, such as color, but especially gloss, as highlighted in Fig. 3. Fig. 3a highlights the color change ΔE of the composite coatings concerning the reference sample P0.0, calculated using the following formula [70]:

$$\Delta E = \left[(\Delta L^*)^2 + (\Delta a^*)^2 + (\Delta b^*)^2 \right]^{1/2} \quad (1)$$

where the colorimetric coordinates L*, a*, and b* represent the lightness (0 for black and 100 for white objects), the red-green axis (positive for red and negative for green), and the yellow-blue axis (positive for yellow and negative for blue), respectively. According to the literature [71], the human eye can perceive a color change greater than one unit. Consequently, it can be stated that the color of samples P0.1 and P1.0 is very

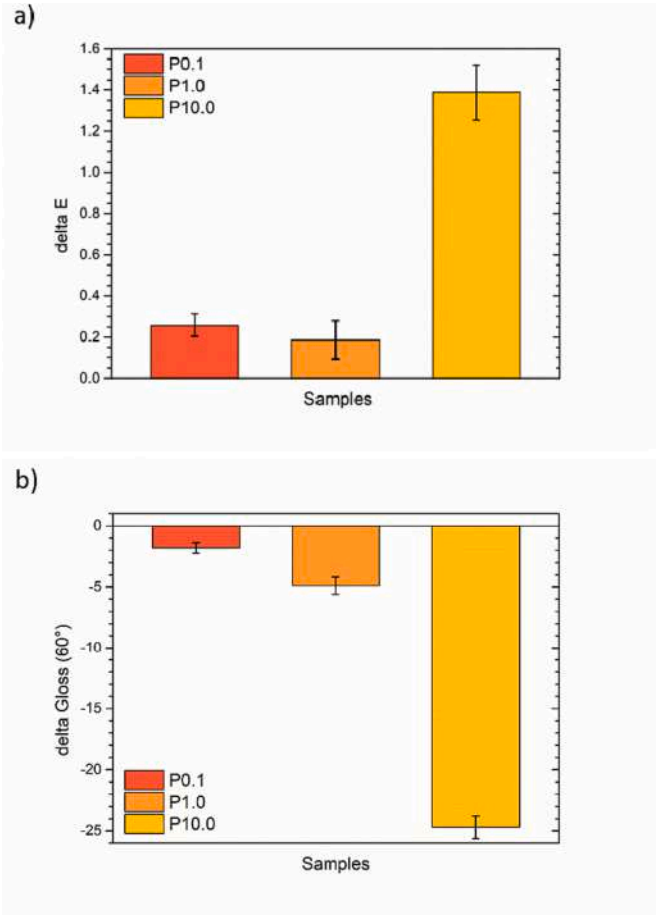

Fig. 3. Evolution of a) color and b) gloss respect to the reference sample P0.0.

similar to that of the reference sample P0.0. Limited quantities of PA11 powders do not significantly affect the color of the protective coating (as they are white-transparent in color). Increased amounts of filler, exemplified in sample P10.0, result in a more pronounced yet still restricted color change ΔE, slightly surpassing unity. Consequently, it would be challenging for humans to discern the coloring impact of the filler. This represents a significant factor since PA11 powders could serve as a functional bio-based additive without posing concerns about altering the desired paint color.

However, the significant aesthetic impact introduced by PA11 powders pertains to the reflective properties of the paint, as depicted in the graph in Fig. 3b, illustrating the changes in gloss values based on the quantity of filler. Starting from an initial gloss value of 31.9, the paint shows a decrease in gloss to 30.1, 27.0, and 7.2 with the gradual addition of PA11 granules for samples P0.1, P1.0, and P10.0, respectively. The inclusion of the filler notably reduces the reflectance of the paint, with sample P10.0 exhibiting a particularly opaque appearance. The literature actually refers to Rilsan® powders as organic substances used for matting purposes [72]. This outcome aligns precisely with the progressive rise in roughness outlined in Table 2. Thus, the incorporation of substantial filler quantities significantly influences the coating's morphology, consequently leading to notable implications for the sample's aesthetic properties.

Definitely, these studies reveal that the powders of PA11 have minimal impact on the specific color of the coating. However, the introduction of the bio-based additive significantly alters the coating's texture, notably increasing its roughness while reducing the gloss of the paint. Consequently, adding PA11 to the paint yields intriguing effects from both a morphological and aesthetic perspective, without directly impacting the coating's color. Therefore, PA11 granules serve as suitable functional fillers for organic coatings, ensuring consistent coloration.

3.2. Coatings mechanical features

3.2.1. Coatings hardness and friction coefficient

Fig. 4 visually displays an example of the impressions formed by the Buchholz indenter on the surfaces of the four coatings. The four images not only emphasize the surface morphology affected by the amount of additive, as previously outlined in Table 2, but they also display imprints from the indenter that vary in appearance based on the sample. These marks seem to reduce in width and length as the concentration of PA11 increases, showcasing possible strengthening and reinforcing effect of the overall coating by the bio-based filler.

Fig. 5 serves as stronger evidence for this pattern, illustrating measurements from the Buchholz hardness test. It shows the average length of the indentations made by the instrument's indenter, correlating directly with the Buchholz hardness value. The acrylic matrix is notably soft, making it prone to indenter penetration. Consequently, the hardness values recorded are relatively low, averaging less than 50 on the Buchholz scale. Indeed, the reinforcing impact of the filler isn't apparent until sample P10.0, where a distinct reduction in the average length of the indenter's footprint becomes noticeable. Consequently, neither 0.1 wt% nor 1.0 wt% of additive proves sufficient to demonstrate a significant increase in hardness. A concentration of 10.0 wt% of PA11 causes a 9.3 % reduction in the average length of the imprints compared to the reference sample, indicating a tangible effect. Prior research has utilized cellulose microfibers [42] to enhance the hardness of acrylic paint for wood. However, these studies noted a low threshold for the filler amount, beyond which the composite coating's performance deteriorates due to unavoidable agglomeration and change of its morphological structure. In contrast, in this case, the linear increase suggests better dispersion of PA11 powders compared to cellulose-based fillers, indicating a more uniform distribution within the coating. Nonetheless, the hardness increase cannot be deemed significant as it still remains below the value of 50 on the Buchholz scale. In essence, PA11 powders do indeed demonstrate higher hardness compared to the pure acrylic matrix of the coating. However, they do not distinctly enhance the system except at concentrations higher than those experimented with in this study.

Nevertheless, a noteworthy hardness, coupled with a notable increase in roughness, makes conceivable that substantial amounts of PA11 might impact factors associated with the friction coefficient of the coating surfaces. Therefore, the impact of various filler concentrations on altering the static friction coefficient of the paint was assessed using the experimental setup depicted in Fig. 6a and previously described in Section 2.3. The static friction coefficient (COF) was determined by the ratio of the minimum tangential force F_T, necessary to initiate motion between the two surfaces in contact (i.e., the sample and the grey cast iron support), divided by the applied normal force, F_N. The tangential force is derived from the product of the mean shear stress, τ_m, needed to separate the contacting asperities, and the actual contact area, A_r [73,74]. Therefore, the coefficient of friction (COF) was represented by the following Eq. (2):

$$COF = \frac{\tau_m * A_r}{F_N} \quad (2)$$

Usually, τ_m is linked to the strength of adhesive bonds formed between the contacting asperities. However, hard and uneven particles can introduce an abrasive element caused by localized plastic deformation phenomena [73,75].

Fig. 6b illustrates the changes in the static friction coefficient concerning the quantity of bio-based additive. The COF values fluctuate, averaging between 0.167 and 0.280, aligning with findings from previous literature on friction and wear characteristics of friction materials [59]. The error bars in Fig. 6b display considerable variability across all four series of samples, which is typical for this type of test and leads to

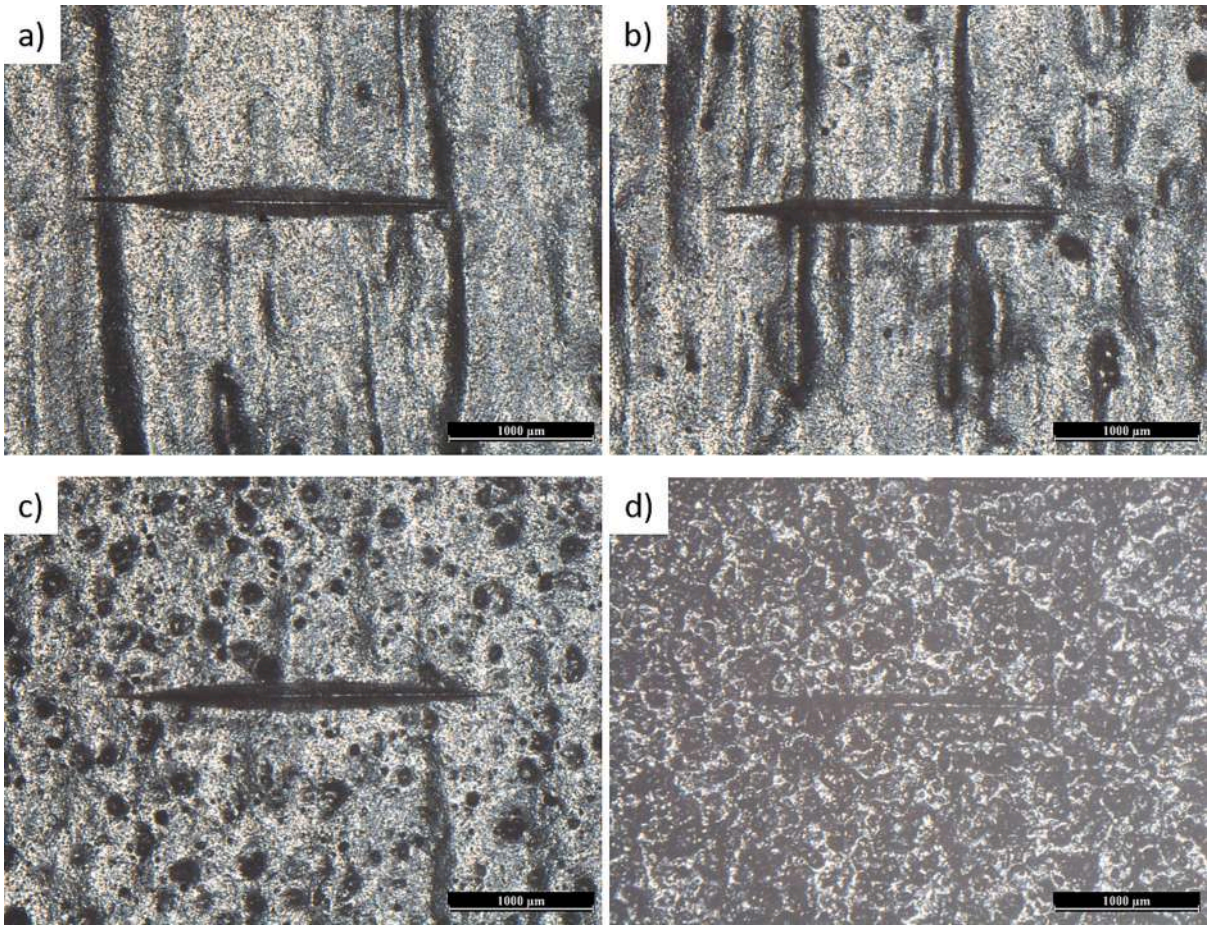

Fig. 4. Optical microscope images of Buchholz test notches on a) sample P0.0, b) sample P0.1, c) sample P1.0 and d) sample P10.0.

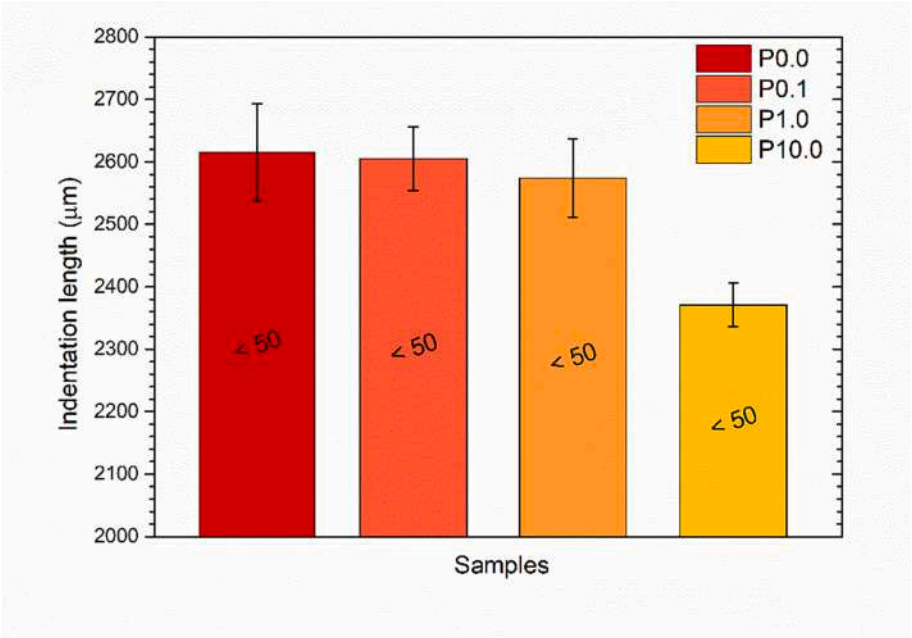

Fig. 5. Average size of indentation imprints in Buchholz hardness testing, accompanied by their corresponding Buchholz hardness outcomes.

some dispersion of results. Nevertheless, despite this dispersion, the average values demonstrate a distinct pattern: a decrease corresponding to the rise in the concentration of PA11 in the paint. Indeed, this outcome is rather surprising since the typical expectation would be for an elevation in COF with the introduction of the bio-based additive, considering its higher hardness compared to the acrylic matrix and its

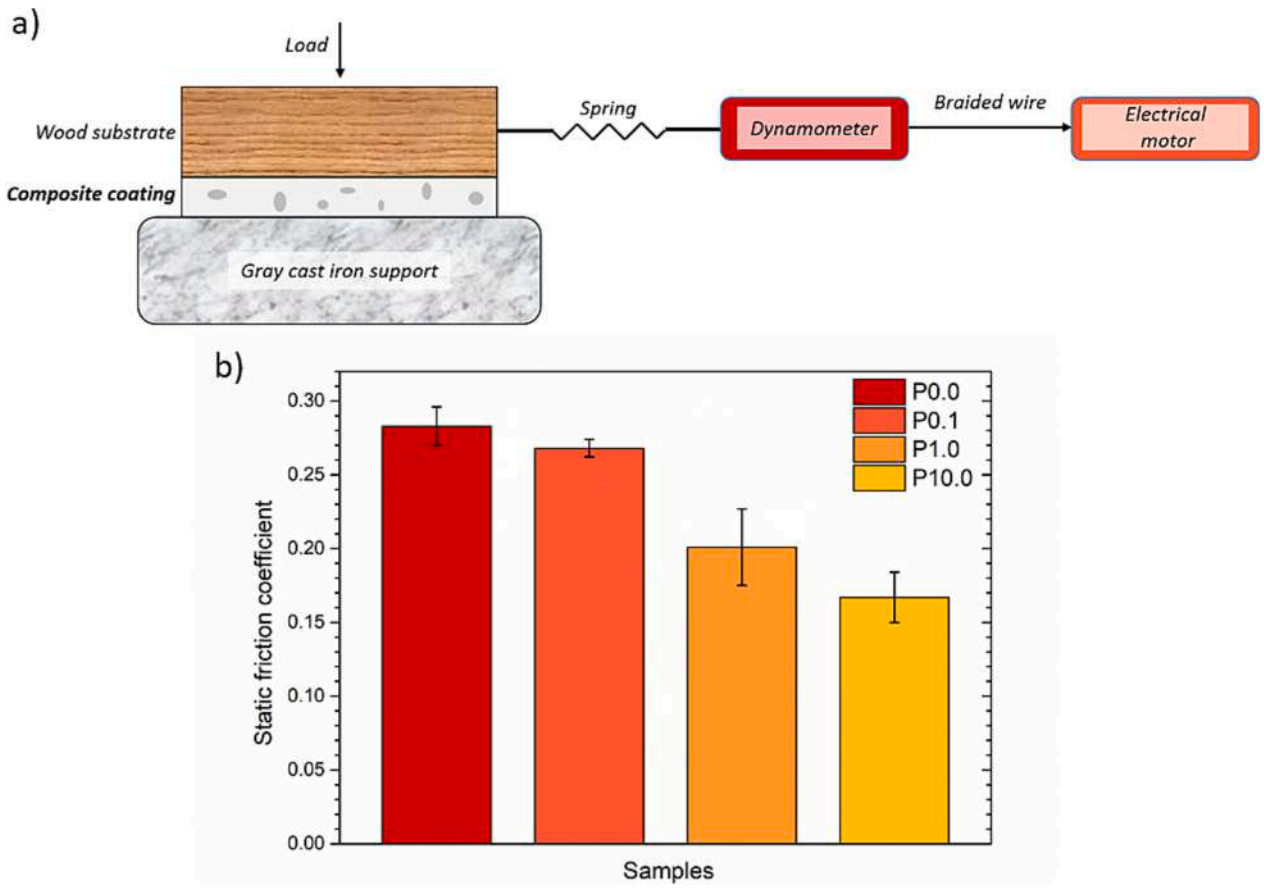

Fig. 6. a) Schematic of the experimental set-up for the measurements of the static friction coefficients (adapted from [58]) and b) the corresponding test outcome.

potential to substantially increase the coating's roughness. The test implies that the additive undergoes significant changes due to the shear stresses it experiences during testing. This phenomenon might somehow promote slippage within the coating. It's worth noting that the asperities present in the P10.0 sample result in a reduction of the actual contact area, A_r, consequently lowering the COF value, as described by the previous Eq. (2).

Hence, to delve deeper into understanding the filler's response to stress and elucidate the atypical friction coefficient test results, the samples underwent varying degrees of abrasive processes. This was done to assess how the PA11 powders react to shear and abrasion stress phenomena.

3.2.2. *Coatings abrasion resistance*

Initially, the samples' resistance to abrasion underwent assessment through notably aggressive evaluations like the Taber test. Fig. 7a emphasizes the test results, showcasing the mass lost per cycle count. The trends observed in the curves of the four types of samples indicate an almost straight-line progression, with a declining slope correlating with increased filler concentration. This suggests that the PA11 powders

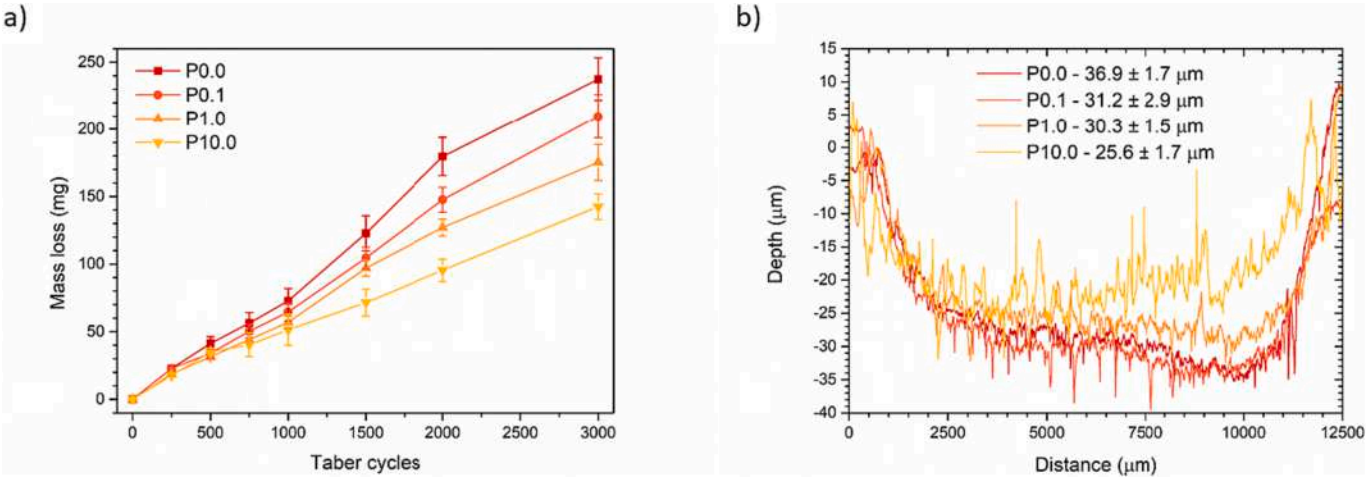

Fig. 7. a) Coatings mass loss, as a function of the Taber cycles and b) profile analysis of the footprint generated by the Taber test (3000 cycles). The values in the legend correspond to the mean maximum depth calculated from 50 measurements for each series (comprising 10 measurements for 5 samples).

contribute to reducing the mass removed by the abrasive wheels in the Taber equipment, ultimately enhancing the composite coating's resistance to abrasion. Following a substantial 3000 Taber cycles, incorporating 0.1 wt%, 1.0 wt%, and 10.0 wt% of PA11 resulted in reduced mass loss compared to the reference sample P0.0. Specifically, the reductions were 11.7 %, 26.2 %, and 40.0 %, respectively. This occurrence correlates with a decrease in the depth of the abrasive impact, as depicted in Fig. 7b. The graph displays a profile analysis of the four coatings after the accelerated degradation test, demonstrating the reduction in abrasive attack depth with the addition of the PA11 powder. Indeed, even a minimal addition of 0.1 wt% of the additive showcases a notable strengthening effect. This effect becomes notably evident

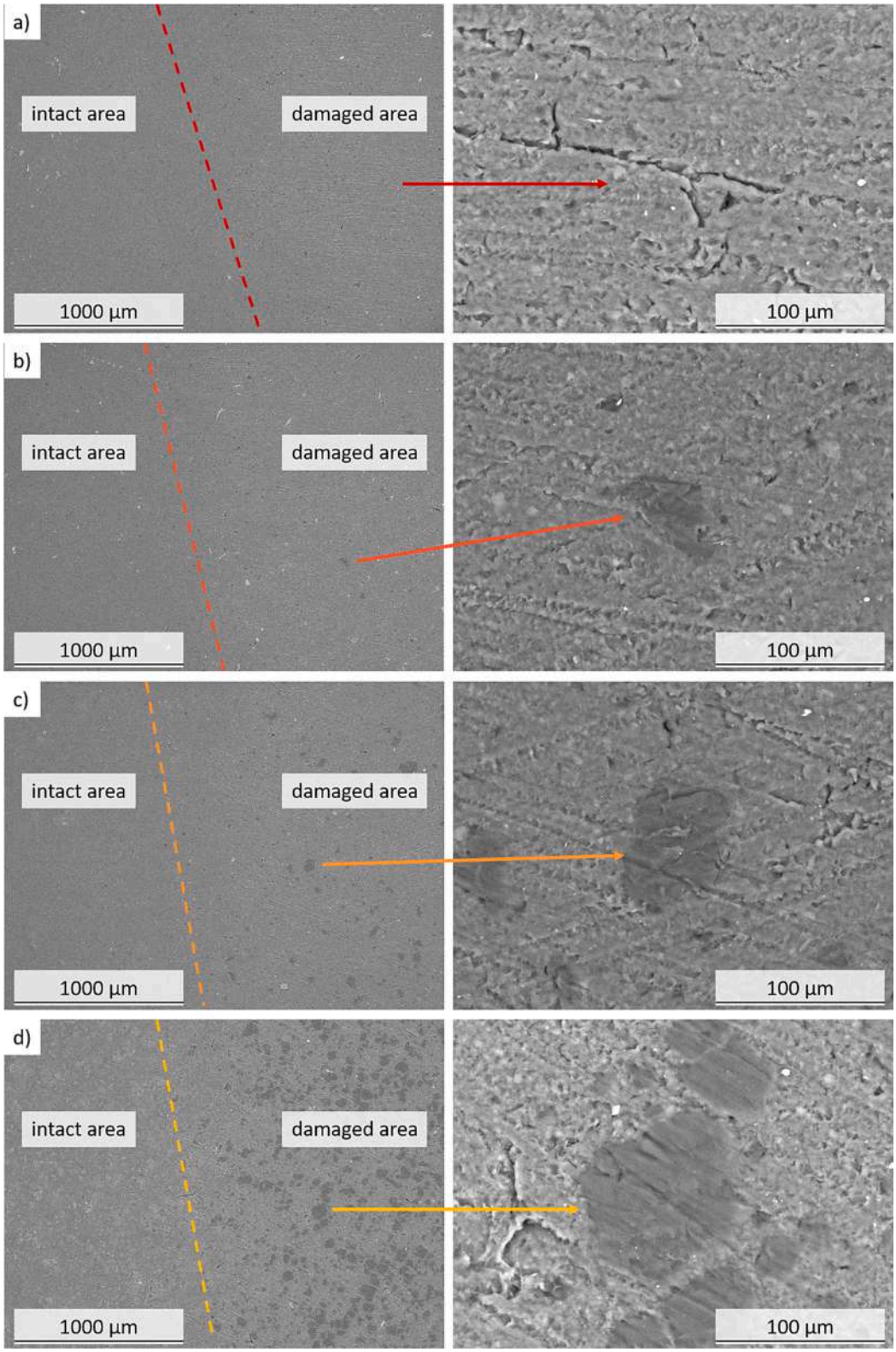

Fig. 8. SEM micrographs of a) sample P0.0, b) sample P0.1, c) sample P1.0 and d) sample P10.0, after 3000 Taber cycles.

in sample P10.0, where the depth of the Taber wheels footprint decreases by approximately 10 μm compared to what was observed in the reference sample P0.0. As with the Buchholz hardness test, paint performance improves with increasing filler content. This is not always true: for example, other works relating to the use of cellulose nanocrystals [27,76] have highlighted how excessive quantities of additive lead to a reduction in the abrasion resistance of acrylic paints for wood, due to agglomerations of the filler. From this perspective, PA11 powders emerge as an excellent filler for acrylic paints. Their ease of dispersion facilitates their utilization in substantial quantities without eliciting adverse effects.

Thus, for a deeper comprehension of the reinforcing filler's behavior, SEM analysis was conducted on the samples' surfaces after the Taber test, illustrated in Fig. 8. The magnified views in the right images emphasize a widespread and uniform impact, evident through distinct abrasion lines caused by the Taber wheels, characteristic of this rigorous test [58,77]. The region affected by the grinding wheels reveals the presence of PA11 granules, appearing as darker spots, notably prominent in sample P10.0. Even after the abrasive test, these granules persist, firmly embedded within the acrylic matrix of the coating. Consequently, the shear stresses didn't result in the complete expulsion of the filler; instead, the notably aggressive phenomenon led to its partial removal. Absolutely, the imprints left by the granules exhibit identical abrasion lines as the surrounding acrylic material, suggesting that the abrasive process didn't distinctly differentiate between the two constituents (filler and matrix) of the coating.

Evidently, the Taber test effectively reveals distinct outcomes among the four series of coatings. However, the intensity of the abrasive attack is so pronounced that it doesn't permit the specific behavior of the PA11 filler to be distinctly discerned. Considering this limitation, the samples underwent characterization using the scrub test, which is a less aggressive abrasive experiment specifically designed for paints [78,79]. Indeed, Fig. 9 demonstrates a result akin to the Taber test depicted in Fig. 7a. Here, as the concentration of the bio-based additive increases, the graph showcases a similar trend of reduced material removal during the abrasive process. In this scenario, the influence of the filler appears less pronounced compared to the results from the Taber test, primarily because the abrasive process is less intense and aggressive in the scrub test. Incorporating 0.1 wt%, 1.0 wt%, and 10.0 wt% of PA11 powder leads to reductions in mass loss amounting to 2.9 %, 10.0 %, and 12.5 %, respectively.

Even with the scrub test's less aggressive nature, it remains possible to recognize the protective function of the filler. Moreover, the SEM observations offer a more detailed description of the mechanism through which PA11 powders mitigate the mass loss during the abrasive process. Fig. 10 presents these findings. All four types of samples display the characteristic straight abrasion lines resulting from the continuous sliding motion of the abrasive sponge used in the scrub test [42,80]. In contrast to the observations from the Taber test shown in Fig. 8, the PA11 fillers exhibit a distinct morphological change following the shear stress induced by the abrasive sponge. In Fig. 10c, and more prominently in Fig. 10d, the presence of the bio-based granules is noticeable, albeit having experienced considerable plastic deformation. The shear stresses don't result in the expulsion or even partial removal of the filler from the acrylic matrix, as observed in the Taber test. Instead, the abrasive sponge induces plastic deformation of the bio-based additive, despite its considerable hardness, causing it to spread and deform on the coating's surface. A similar phenomenon has been previously documented in studies that utilized wax-based additives to enhance the abrasion resistance of wood paints [47,49]. The scrub pad's action tends to scatter the filler, thereby diminishing the friction between the coating surface and the pad itself. Consequently, the reinforcing effect of the bio-based additive emerges from its capacity to undergo plastic deformation, thereby alleviating surface friction effects. As a result, the coating experiences decreased material loss since it isn't entirely displaced by the pad but rather distributed across the surface of the composite layer. Indeed, this phenomenon not only showcases the filler's protective role in minimizing material removal from abrasive processes but also offers a clearer explanation for the results of the friction coefficient test depicted in Fig. 6b. The filler's plastic deformation serves a dual purpose: enhancing the coating's abrasion resistance and concurrently reducing its static friction coefficient. The increase in PA11 quantity on the surface amplifies the plastic deformation phenomenon, leading to the creation of a smoother and slippery surface that demonstrates a markedly reduced friction coefficient. Consequently, the results depicted in Fig. 6b, illustrating the friction coefficient test, are well-founded. They showcase a progressive decline in the friction coefficient correlating with the rise in PA11 content within the coating.

Absolutely, the strengthening observed with PA11 powders during the Taber test is indeed a result of the filler absorbing energy, leading to

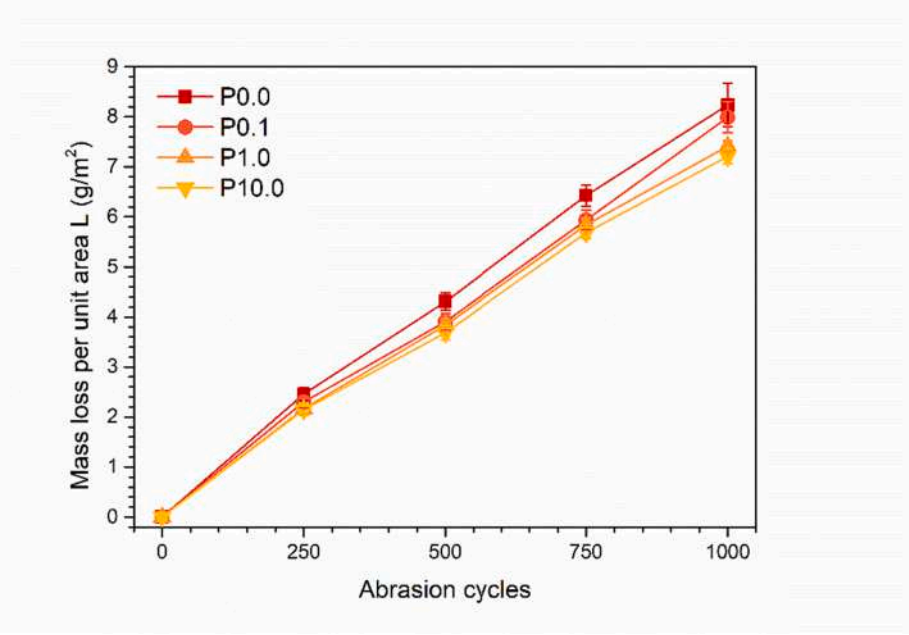

Fig. 9. Loss of coating mass per unit area, as a function of the scrub abrasion cycles.

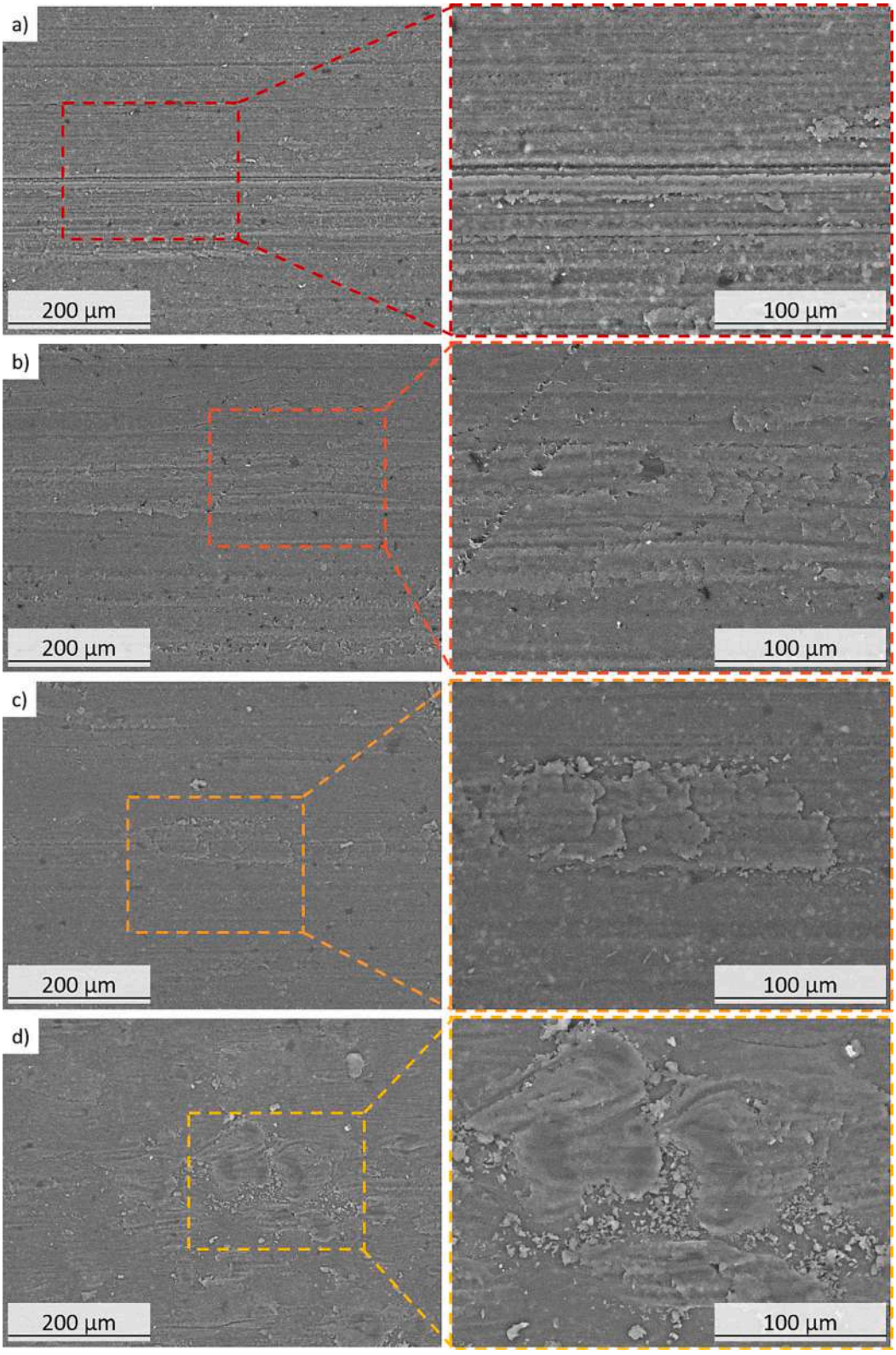

Fig. 10. SEM micrographs of a) sample P0.0, b) sample P0.1, c) sample P1.0 and d) sample P10.0, after 1000 scrub cycles.

its partial removal. This phenomenon is accompanied by a noticeable slippery effect, which becomes more apparent in the results of the scrub test. Additionally, owing to the lower density of the filler compared to the acrylic matrix, the sample with higher PA11 content experiences lower weight loss for an equivalent amount of material removed. Altogether, these diverse tests focused on abrasion and surface properties have effectively showcased the protective capabilities of PA11 powder, primarily achieved through the plastic deformation of the filler.

While the slippery effect is less pronounced compared to the use of actual waxes [47,49], PA11 still demonstrates potential. Incorporating hard particles like silica [81], ductile flakes of stainless steel [82] or low energy surface hollow glass microspheres [83] could enhance mass

reduction, but PA11 proves to be an excellent compromise in terms of cost-effectiveness, performance, and eco-friendly attributes.

Additionally, the aforementioned micrometric mechanical phenomena induce a notable aesthetic alteration in the coatings, a change accentuated in the graphs presented in Fig. 11. The dispersion of the filler, coupled with the abrasion process affecting the acrylic matrix, results in a consistent decrease in gloss values (Fig. 11a). This reduction is more pronounced in samples that initially exhibited higher reflectance, notably seen in P0.0 and P0.1. Absolutely, the observed decline in gloss correlates with a shift in the coating's roughness (Fig. 11b), particularly noticeable in samples containing higher PA11 content. While abrasion of the acrylic matrix notably elevates the R_z values, as seen in samples P0.0 and P0.1, the plastic deformation of the filler, resulting in the flattening of surface agglomerates (as previously depicted in Fig. 2d), causes a reduction in R_z specifically in sample P10.0. Overall, the filler demonstrates not only a protective role but also significant aesthetic durability, as the initially low gloss values are not notably affected by the abrasive process. Ultimately, the removal of material induced by the scrub test, leading to increased roughness of the acrylic matrix, is visibly pronounced in the P0.0 sample. In contrast, visually inspecting the P10.0 sample doesn't indicate such an intense abrasive attack.

Definitely, the PA11 powder provides a tangible protective effect by reducing mass loss due to abrasion. This bio-based additive goes beyond merely acting as an anti-abrasion filler; it enhances the mechanical properties of the acrylic matrix, decreases the static friction coefficient, and preserves the coating's long-term durability and aesthetic appeal.

3.3. Coatings liquid resistance

Different quantities of the bio-derived additive were examined to understand how they affected the barrier characteristics of the acrylic matrix through various tests. The results of the cold liquid resistance test are depicted in Fig. 12, which indicates the color change values, denoted as ΔE, subsequent to the interaction between the coatings and the four test solutions. As anticipated, substances like NaCl, ethanol, and detergent solutions typically do not induce significant color alterations in the coating, thereby resulting in ΔE values that align with category 0 as per the standard [84]. Even with an equivalent additive content, these outcomes surpass previous studies involving the incorporation of photochromic microcapsules in acrylic paints for wood [85]. This underscores the remarkable resilience of the bio-based filler, even at higher concentrations as observed in sample P10.0, against standard solutions. On the contrary, among the four substances tested, red ink consistently induces the most pronounced color alteration in the coating [48]. Specifically, the four sets of samples display ΔE values corresponding to categories 4–5, representing the highest range of color change as per the standard. As the concentration of PA11 powders increases, the chromatic modification becomes more pronounced. This implies a defectiveness introduced into the coating by the bio-based filler, facilitating a more straightforward percolation of the test coloring solution.

The micrographs displayed in Fig. 13 offer a clearer insight into this phenomenon. In contrast to the acrylic matrix, which displays a generally uniform albeit weakened absorption of the ink, the presence of substantial amounts of PA11 reveals intense coloring concentrated in specific areas (Fig. 13d). These colored spots correspond to the PA11 granules situated close to the coating surface. These granules tend to absorb color more readily, potentially due to a suboptimal interface with the acrylic matrix that promotes the ink percolation. On a larger macroscopic scale, this phenomenon results in a more prominent color alteration, reaching a grade 5 according to the standard's classification. Nonetheless, this result might predominantly stem from the presence of larger surface granules, contributing to increased roughness in the P10.0 sample. Indeed, their propensity to absorb ink color is a crucial aspect, particularly evident when there's a high concentration of additive near the outer surface of the coating, as seen in sample P10.0. However, the incorporation of PA11-based fillers doesn't inherently guarantee a decline in the barrier performance or hydrophobic characteristics of the acrylic matrix.

Thus, to comprehensively examine the macroscopic barrier properties of the four coatings, the samples underwent characterization through the liquid water uptake test. This test involved monitoring the absorption of water by the composite layers over a specified period. Fig. 14 illustrates the test outcomes, depicting the water uptake over a 100-h period of contact between the coatings' surface and water. The graph compares the performance of the four coatings with that of an uncoated wood sample, emphasizing the significance of the protective layer. The untreated wooden panel absorbs a substantial amount of water within the initial 6 h of testing, followed by a slower rate of absorption until it nearly reaches saturation. In contrast, the four sample types display a comparable pattern but with significantly lower water absorption, indicating a strong barrier effect offered by the coatings. Overall, there's no notable distinction among the behavior of the four coatings. This is a crucial but frequently overlooked aspect: the introduction of different fillers into acrylic paints has often led to a reduction in the paint's barrier effect, mainly due to the hydrophilic nature of the additive [86,87]. However, in this instance, the presence of the powder of PA11 does not compromise the barrier characteristics of the polymer matrix. Yet, a slight reduction in water uptake is noticeable with higher filler concentrations. This outcome appears contradictory to the cold liquid resistance test results, which pointed to an easier percolation of the test solution due to the interaction between the bio-based additive and the acrylic matrix.

Even in this scenario, the influence of the filler on the coating's

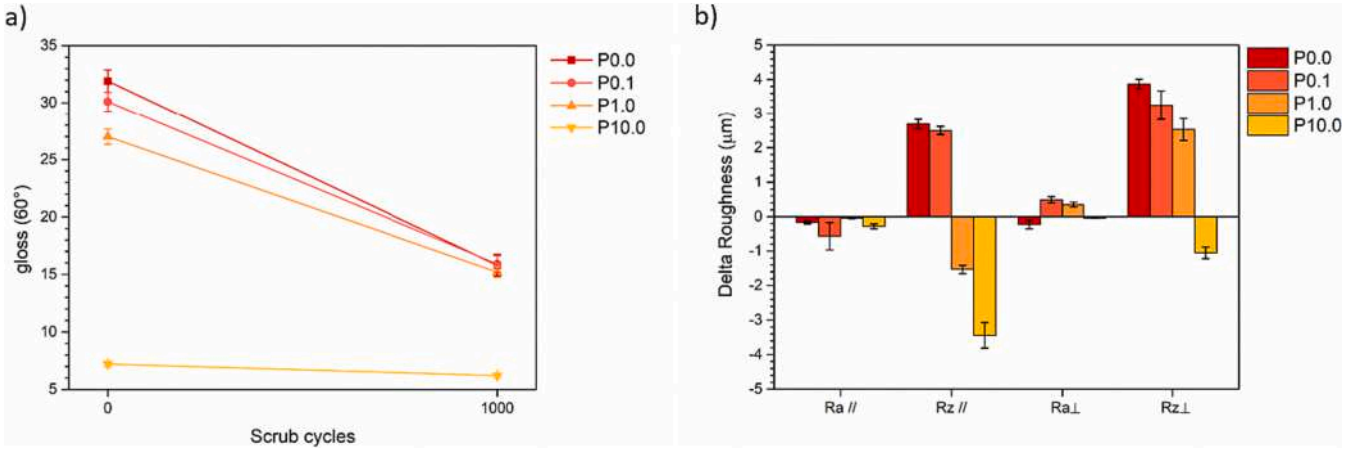

Fig. 11. Evolution of a) gloss and b) roughness after the scrub test.

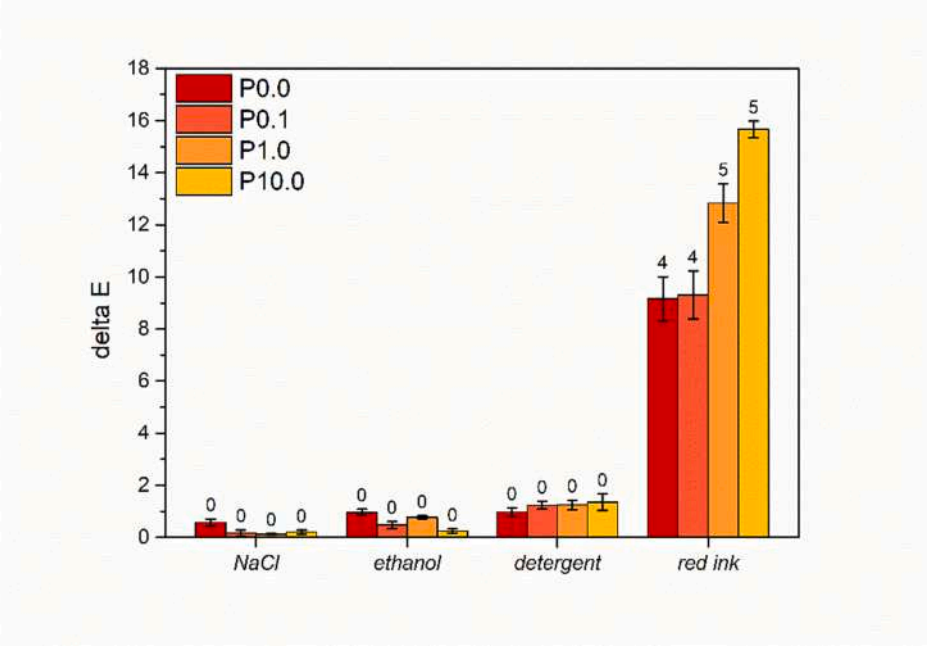

Fig. 12. Color variation of the samples after the liquid resistance test. The numbers displayed above the columns reflects the discoloration levels described in [84].

morphology affects its hydrophobic performance. Indeed, it's important to note that PA11, in contrast to other polyamides, demonstrates heightened hydrophobic characteristics owing to a lower frequency of amide groups in its polymer chain, resulting in a less polar polymer structure [88]. Consequently, contact angle measurements were conducted to assess the genuine hydrophilic/hydrophobic characteristics of the coatings. The wettability test results are outlined in Table 3, and Fig. 15 exhibits images captured during the measurements, demonstrating the behavior of the four samples. Fig. 15a, b, and c display drops with highly similar characteristics. Specifically, the three samples - P0.0, P0.1, and P1.0 - exhibit comparable average contact angle values. This similarity indicates the limited impact of small amounts of PA11 powder on altering the wettability characteristics of the acrylic matrix. In contrast, Fig. 15d showcases a drop with a notably larger contact angle compared to the previous three samples. High concentrations of the bio-based additive demonstrate the capability to enhance the hydrophobicity of the composite coating. Nevertheless, with contact angle values around 59°, which are still relatively low, attributing purely hydrophobic properties to the P10.0 sample isn't conclusive [89]. However, the noteworthy increase in contact angle owing to the presence of PA11 powders remains significant. The rise in contact angle is not primarily due to inherent hydrophobic properties within the additive; moreover, the additive has been demonstrated to facilitate solution absorption within the coating. Instead, this increase is largely a consequence of the significant elevation in surface roughness introduced by the abundance of powders (as indicated in Table 2). Consequently, the substantial rise in roughness effectively counteracts the shortcomings arising from the interface between the filler and matrix, leading to a slightly enhanced hydrophobic performance on the surface of sample P10.0. However, this improvement isn't evident at a macroscopic level, such as in tests assessing resistance to liquids or water uptake. Instead, it's primarily influenced by the extent of local roughness.

In summary, the PA11 powder stimulates distinct percolation and solution absorption within the acrylic matrix of the coating. However, at a macroscopic level, there aren't notable differences observed regarding the surface wettability. This is due to two opposing phenomena: defects and heightened roughness resulting from substantial additive content. The combination of these factors suggests that the bio-based additive can be incorporated in significant quantities without manifesting particular macroscopic effects on the coating's barrier properties.

3.4. Coatings outdoor durability

Recent studies delved into the influence of functional fillers and bio-based pigments on the protective qualities of wood paints [42,44,48,49]. These investigations evaluated paint durability using accelerated degradation tests, including UV-B and UV-A exposure, coupled with infrared spectroscopy FTIR analysis. However, the effectiveness of this analysis method was limited due to the strong UV resistance of acrylic paint, making it challenging to pinpoint specific degradation effects. Consequently, this research relied on straightforward colorimetric and gloss analyses to gauge potential sample degradation. To simulate solar radiation exposure more realistically, the study used xenon lamps for accelerated testing, opting for a less aggressive but more representative approach compared to UV-A and UV-B radiation.

Fig. 16a showcases the evolution of color change (ΔE) observed during the accelerated degradation test of the three samples. This change is contrasted with the behavior of a wooden panel, serving as an added reference to highlight the paint's protective role. Notably, the poplar wood displays a swift and substantial color alteration, mainly due to the rapid breakdown of its main components—cellulose, hemicellulose, and lignin—resulting in noticeable yellowing of the sample. The color change observed in the reference sample P0.0 is relatively minor, approximately 2 units. This change doesn't stem from a physical-chemical breakdown of the acrylic coating but rather from a slight yellowing of the wooden panel itself. The acrylic paint plays a significant role in curbing the degradation of the underlying wood, given its inherent ability to resist solar radiation—a trait well-documented in prior research [90,91]. Moreover, a recent study [92] highlighted that transparent acrylic wood paints don't exhibit aesthetic alterations when applied to surfaces that don't undergo color changes upon UV radiation exposure. Consequently, the paint can only partially alleviate wood deterioration effects. Moreover, due to the paint's transparency, any color alteration induced by the xenon lamp radiation on the wood substrate remains visible. Similarly, the three coatings incorporating the bio-based additive show minimal color alteration. This suggests that PA11 powders remain unaffected by exposure to aggressive radiation, evidenced by the outcome of the P10.0 sample being comparable to that

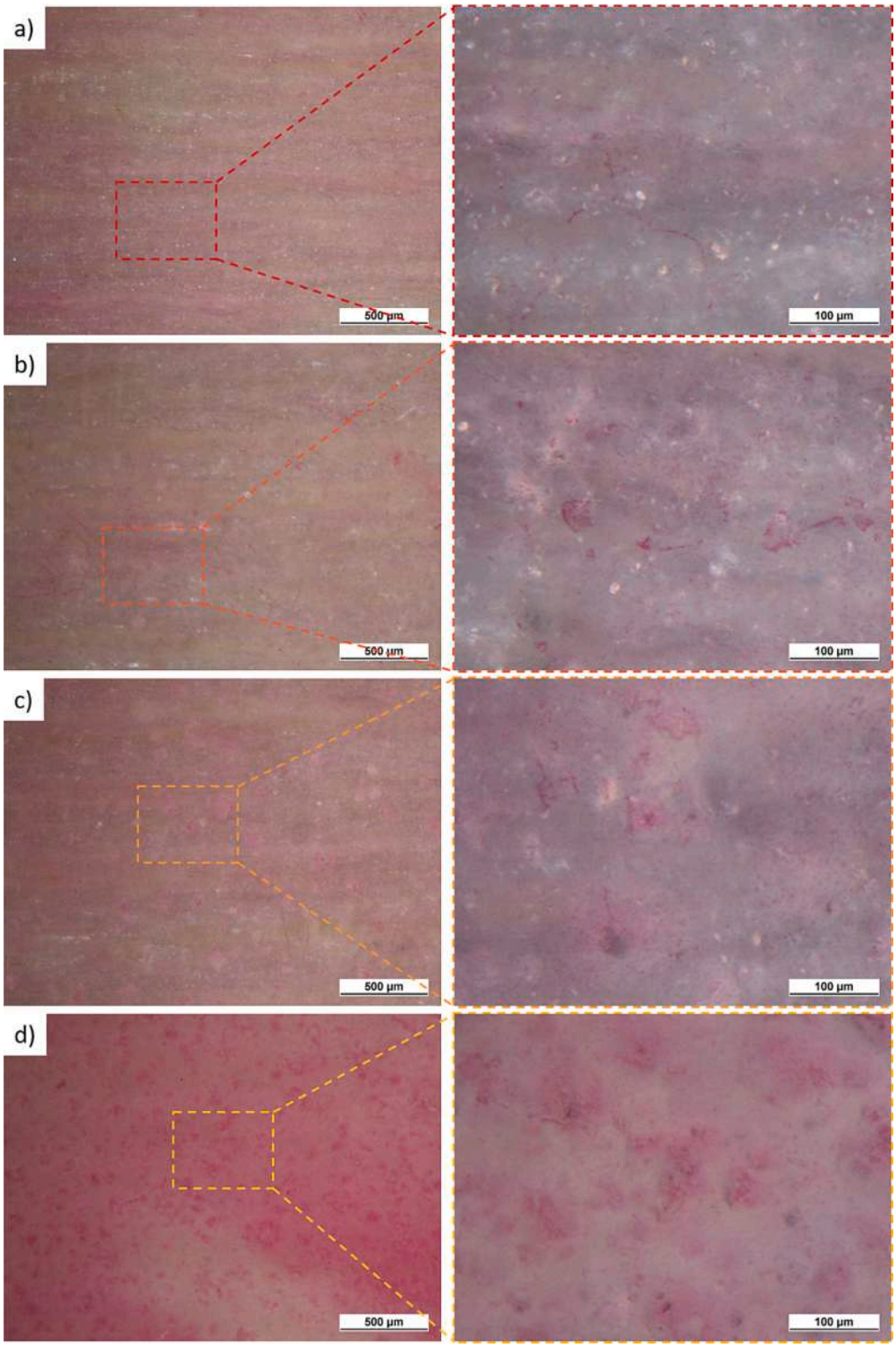

Fig. 13. Optical micrographs of the surface of a) sample P0.0, b) sample P0.1, c) sample P1.0 and d) sample P10.0 after the contact with the red ink. (For interpretation of the references to color in this figure legend, the reader is referred to the web version of this article.)

of the pure acrylic matrix (P0.0). These performances align with those of additives explicitly formulated to mitigate photooxidation in acrylic wood paints, such as UV absorbers and micronized TiO_2 [93], or nanopowders like ZnO and SiO_2 [94].

Contrarily, the four sets of samples showcase a progression in gloss that notably relies on the quantity of bio-based additive, as emphasized in Fig. 16b. The acrylic matrix demonstrates a noticeable decrease in gloss. Nonetheless, this impact lessens with higher concentrations of PA11 powder. However, this doesn't suggest that the filler enhances the aesthetic longevity of the coating: all samples experience a gloss reduction, particularly noticeable in samples with lower filler content due to their initially higher reflectance values. In essence, it's plausible to associate a poor impact of xenon radiation on the gloss of sample P10.0, given its initially lower gloss values (around 7.2° compared to the

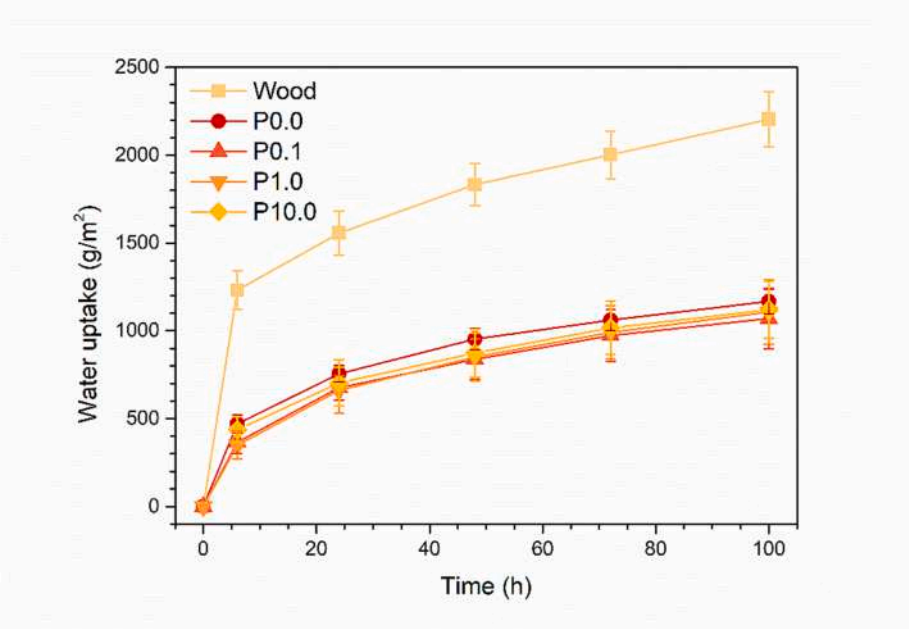

Fig. 14. Tracking of the water uptake by the coatings.

Table 3
Contact angle measurements (θ) carried out with demineralized water.

Sample	Θ (°)
P0.0	51.6 ± 2.2
P0.1	52.8 ± 4.1
P1.0	50.6 ± 5.7
P10.0	59.3 ± 5.6

31.2° of the pure acrylic matrix's). Nonetheless, it's evident that any potential deterioration of the acrylic matrix is effectively concealed by significant amounts of filler and the resulting lower reflectance values.

In summary, the acrylic paint showcases commendable chemical resistance against Xenon radiation, effectively slowing down the photo-oxidation degradation of the wooden substrate to a certain degree. Nonetheless, the paint's transparency highlights the yellowing of the wood. Conversely, PA11 powder displays resilience during accelerated degradation testing, resulting in minimal gloss reduction and thereby maintaining the visual appeal of the sample. Hence, the bio-based additive's durability and aesthetic qualities remain preserved for outdoor use, even when the painted component is directly exposed to solar radiation.

4. Conclusions

This study seeks to examine how various concentrations of PA11 powder affect both the aesthetic appeal and multifunctional capabilities of an acrylic wood paint. The investigations demonstrate that PA11 powders have little effect on the specific color of the coating. However, the incorporation of the bio-based additive notably changes the texture of the coating, increasing its roughness significantly and simultaneously decreasing the paint's gloss.

Conversely, the bio-based additive exerts a significant influence on the mechanical properties of the acrylic matrix. It slightly enhances the hardness of the coating but more notably reduces its friction coefficient. This particular phenomenon primarily stems from a plastic deformation effect of the granules, which further contributes to diminishing material removal during abrasive processes. This phenomenon becomes evident through aggressive abrasion tests like the Taber test and milder ones like the scrub test. Additionally, the coating with higher PA11 content is less affected by abrasion processes. Its notably low gloss values remain largely unaffected by shear stresses and material removal.

Additionally, the PA11 powder prompts distinctive percolation and absorption within the acrylic matrix of the coating. However, at a macroscopic level, there aren't significant differences observed in terms of surface wettability. This is attributed to two conflicting phenomena: new defectiveness and increased roughness resulting from substantial additive content. The interplay of these factors implies that the bio-based additive can be integrated in considerable amounts without displaying notable macroscopic effects on the coating's barrier properties.

Finally, PA11 powder exhibits good durability under accelerated degradation testing, leading to minimal gloss reduction and thus preserving the visual appeal of the sample. Therefore, the durability and aesthetic attributes of the bio-based additive persist for outdoor applications, even when the painted component is directly subjected to solar radiation.

In conclusion, among the studied PA11 contents, 10 wt% emerges as the most optimal. Despite substantially decreasing the coating's gloss, the elevated proportion of this eco-friendly additive notably diminishes the friction coefficient, substantially enhancing the coating's abrasion resistance. Additionally, it effectively sustains high aesthetic durability when subjected to solar radiation. The remarkable outcomes achieved with substantial concentrations of PA11 hint at potential future explorations. These investigations could delve into the behavior of higher quantities of filler to ascertain a potentially optimal concentration surpassing the 10 wt%.

Considering all these facets, it's sensible to regard PA11 powder as a promising standard in the progression of composite coatings for versatile applications in woodworking industries, which requires durability over time and remarkable mechanical strength.

Funding

This research did not receive any specific grant from funding agencies in the public, commercial, or not-for-profit sectors.

CRediT authorship contribution statement

Massimo Calovi: Writing – original draft, Validation, Methodology,

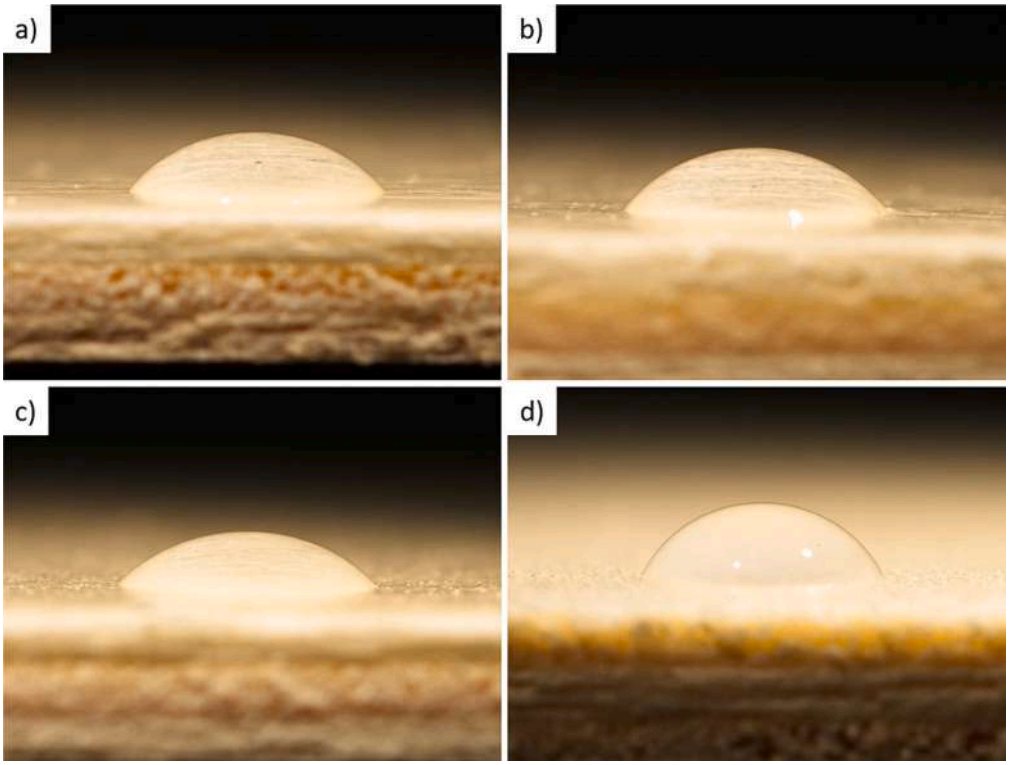

Fig. 15. Optical micrograph of the contact angle measurements carried out with demineralized water of a) sample P0.0, b) sample P0.1, c) sample P1.0 and d) sample P10.0.

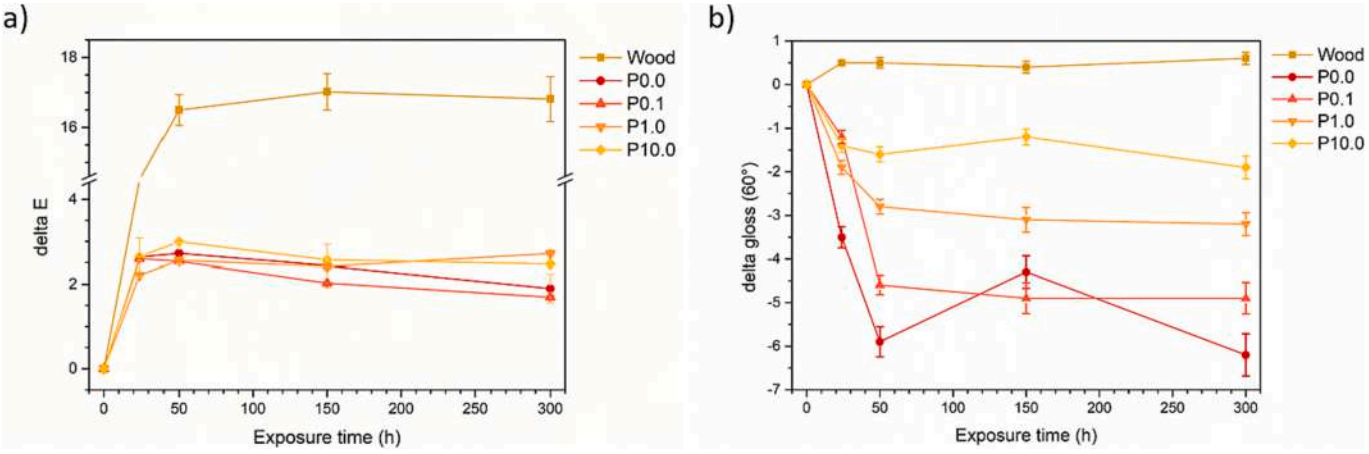

Fig. 16. Changes in a) color and b) gloss of the samples observed throughout the Xenon exposure test.

Investigation, Data curation, Conceptualization. **Stefano Rossi:** Writing – review & editing, Supervision, Resources, Project administration.

Declaration of competing interest

The authors declare that they have no known competing financial interests or personal relationships that could have appeared to influence the work reported in this paper.

Data availability

Data will be made available on request.

Acknowledgments

The authors greatly acknowledge the contributions of Stefano Di Blase (ICA Group, Civitanova Marche, MC, Italy) and Sergi Borsani and Andrea Mannella (Grolman Group, Merate, MB, Italy) regarding the paint and the PA11 powders supply, respectively. The publication was created with the co-financing of the European Union – FSE-REACT-EU, PON Research and Innovation 2014–2020 DM1062/2021.

Appendix A. Supplementary data

Supplementary data to this article can be found online at https://doi.org/10.1016/j.porgcoat.2024.108262.

References

[1] R. Willemen, H. Verstraelen, R. Meskens, D. Luyckx, K. Vastmans, S. Lenaerts, G. Potters, K. De Baere, The economics of a long term coating, international journal of, Marit. Eng. 159 (2017).
[2] J. Davis, The effects and economic impact of corrosion, in: Corrosion: Understanding the Basics, ASM International Almere, The Netherlands, 2000, pp. 62–66.
[3] A.S. Khanna, High-Performance Organic Coatings, Elsevier, 2008.
[4] U. Kopacz, New Trends in Decorative Coatings, Metal Finishing(USA) 90, 1992, pp. 7–10.
[5] S.G. Kandi, B. Panahi, N. Zoghi, Impact of surface texture from fine to coarse on perceptual and instrumental gloss, Prog. Org. Coat. 171 (2022) 107028.
[6] A.S.H. Makhlouf, Handbook of Smart Coatings for Materials Protection, Elsevier, 2014.
[7] L. Wu, X. Guo, J. Zhang, Abrasive resistant coatings—a review, Lubricants 2 (2014) 66–89.
[8] Z. Yuxuan, Z. Yunyun, Y. Jianrong, Z. Xiaoqiang, Energy saving performance of thermochromic coatings with different colors for buildings, Energ. Buildings 215 (2020) 109920.
[9] L.Y. Wu, Q. Zhao, H. Huang, R. Lim, Sol-gel based photochromic coating for solar responsive smart window, Surf. Coat. Technol. 320 (2017) 601–607.
[10] T. Wei, Y. Qu, Y. Zou, Y. Zhang, Q. Yu, Exploration of smart antibacterial coatings for practical applications, Curr. Opin. Chem. Eng. 34 (2021) 100727.
[11] A. Baldelli, J. Ou, D. Barona, W. Li, A. Amirfazli, Sprayable, superhydrophobic, electrically, and thermally conductive coating, Adv. Mater. Interfaces 8 (2021) 1902110.
[12] S. Naghdi, K.Y. Rhee, D. Hui, S.J. Park, A review of conductive metal nanomaterials as conductive, transparent, and flexible coatings, thin films, and conductive fillers: different deposition methods and applications, Coatings 8 (2018) 278.
[13] M.S. Mozumder, A.-H.I. Mourad, H. Pervez, R. Surkatti, Recent developments in multifunctional coatings for solar panel applications: a review, Sol. Energy Mater. Sol. Cells 189 (2019) 75–102.
[14] X. Lu, Z. Wu, K. Xu, X. Wang, S. Wang, H. Qiu, X. Li, J. Chen, Multifunctional coatings of titanium implants toward promoting osseointegration and preventing infection: recent developments, Front. Bioeng. Biotechnol. 9 (2021) 783816.
[15] M.F. Montemor, Functional and smart coatings for corrosion protection: a review of recent advances, Surf. Coat. Technol. 258 (2014) 17–37.
[16] S. Rossi, F. Russo, M. Calovi, Durability of vitreous enamel coatings and their resistance to abrasion, chemicals, and corrosion: a review, Journal of Coatings Technology and Research 18 (2021) 39–52.
[17] S.B. Ulaeto, R. Rajan, J.K. Pancrecious, T. Rajan, B. Pai, Developments in smart anticorrosive coatings with multifunctional characteristics, Prog. Org. Coat. 111 (2017) 294–314.
[18] J. Radkau, Wood: A History, Polity Press, Cambridge, 2012.
[19] J.K. Kim, K. Pal, Recent Advances in the Processing of Wood-Plastic Composites, Springer-Verlag, Berlin Heidelberg, 2010.
[20] R.B. Hoadley, Chemical and Physical Properties of Wood, the Structural Conservation of Panel Paintings: Proceedings, Part 1:, Wood Science and Technology, 1998, pp. 2–20.
[21] J. Hao, X. Wu, G. Oporto, W. Liu, J. Wang, Structural analysis and strength-to-weight optimization of wood-based sandwich composite with honeycomb core under three-point flexural test, European Journal of Wood and Wood Products 78 (2020) 1195–1207.
[22] M. Pánek, L. Reinprecht, Colour stability and surface defects of naturally aged wood treated with transparent paints for exterior constructions, Wood Res 59 (2014) 421–430.
[23] F. Zareanshahraki, V. Mannari, Formulation and optimization of radiation-curable nonisocyanate polyurethane wood coatings by mixture experimental design, Journal of Coatings Technology and Research 18 (2021) 695–715.
[24] R. Bansal, S. Nair, K.K. Pandey, UV resistant wood coating based on zinc oxide and cerium oxide dispersed linseed oil nano-emulsion, Materials Today Communications 30 (2022) 103177.
[25] V. Jirouš-Rajković, J. Miklečić, Enhancing weathering resistance of wood—a review, Polymers 13 (2021) 1980.
[26] S. Veigel, G. Grüll, S. Pinkl, M. Obersriebnig, U. Müller, W. Gindl-Altmutter, Improving the mechanical resistance of waterborne wood coatings by adding cellulose nanofibres, React. Funct. Polym. 85 (2014) 214–220.
[27] P. Hochmańska-Kaniewska, D. Janiszewska, T. Oleszek, Enhancement of the properties of acrylic wood coatings with the use of biopolymers, Prog. Org. Coat. 162 (2022) 106522.
[28] S.M. Miri Tari, A. Tarmian, M. Azadfallah, Improving fungal decay resistance of solvent and waterborne polyurethane-coated wood by free and microencapsulated thyme essential oil, J. Coat. Technol. Res. (2022) 1–8.
[29] M. Nikolic, J.M. Lawther, A.R. Sanadi, Use of nanofillers in wood coatings: a scientific review, Journal of Coatings Technology and Research 12 (2015) 445–461.
[30] C.M. Pacheco, B.A. Cecilia, G. Reyes, C. Oviedo, A. Fernández-Pérez, M. Elso, O. J. Rojas, Nanocomposite additive of SiO_2/TiO_2/nanocellulose on waterborne coating formulations for mechanical and aesthetic properties stability on wood, Materials Today Communications 29 (2021) 102990.
[31] J. Janesch, I. Czabany, C. Hansmann, A. Mautner, T. Rosenau, W. Gindl-Altmutter, Transparent layer-by-layer coatings based on biopolymers and CeO^2 to protect wood from UV light, Prog. Org. Coat. 138 (2020).
[32] A.M. Cheumani Yona, J. Žigon, A. Ngueteu Kamlo, M. Pavlič, S. Dahle, M. Petrič, Preparation, surface characterization, and water resistance of silicate and sol-silicate inorganic–organic hybrid dispersion coatings for wood, Materials 14 (2021) 3559.
[33] J. Yang, H. Li, Z. Yi, M. Liao, Z. Qin, Stable superhydrophobic wood surface constracting by KH580 and nano-Al_2O_3 on polydopamine coating with two process methods, Colloids and Surfaces A: Physicochemical and Engineering Aspects 637 (2022) 128219.
[34] H. Zou, S. Wu, J. Shen, Polymer/silica nanocomposites: preparation, characterization, properties, and applications, Chem. Rev. 108 (2008) 3893–3957.
[35] X. Duan, S. Liu, E. Huang, X. Shen, Z. Wang, S. Li, C. Jin, Superhydrophobic and antibacterial wood enabled by polydopamine-assisted decoration of copper nanoparticles, Colloids Surf. A Physicochem. Eng. Asp. 602 (2020) 125145.
[36] L. Cheng, S. Ren, X. Lu, Application of eco-friendlywaterborne polyurethane composite coating incorporated with nano cellulose crystalline and silver nano particles on wood antibacterial board, Polymers 12 (2020).
[37] P.K. Sadh, S. Duhan, J.S. Duhan, Agro-industrial wastes and their utilization using solid state fermentation: a review, Bioresources and Bioprocessing 5 (2018) 1–15.
[38] M. Sanjay, P. Madhu, M. Jawaid, P. Senthamaraikannan, S. Senthil, S. Pradeep, Characterization and properties of natural fiber polymer composites: a comprehensive review, J. Clean. Prod. 172 (2018) 566–581.
[39] R. Mustapha, A.R. Rahmat, R. Abdul Majid, S.N.H. Mustapha, Vegetable oil-based epoxy resins and their composites with bio-based hardener: a short review, Polymer-Plastics Technology and Materials 58 (2019) 1311–1326.
[40] E. Sansonetti, D. Cîrule, E. Kuka, I. Andersone, B. Andersons, Investigation of Linseed Oil Based Wood Coatings: Effect of Artificial Weathering, Key Engineering Materials, Trans Tech Publ, 2019, pp. 223–227.
[41] C.A. Teaca, D. Roşu, F. Mustaţă, T. Rusu, L. Roşu, I. Roşca, C.-D. Varganici, Natural bio-based products for wood coating and protection against degradation: a review, BioResources 14 (2019) 4873–4901.
[42] M. Calovi, S. Rossi, Impact of high concentrations of cellulose fibers on the morphology, Durability and Protective Properties of Wood Paint, Coatings 13 (2023) 721.
[43] S. Tamantini, S. Bergamasco, F. Zikeli, M. Humar, M. Cavalera, M. Romagnoli, Cellulose nano crystals (CNC) as additive for a bio-based waterborne acrylic wood coating: decay, Artificial Weathering, Physical and Chemical Tests, Nanomaterials 13 (2023) 442.
[44] M. Calovi, S. Rossi, From wood waste to wood protection: new application of black bio renewable water-based dispersions as pigment for bio-based wood paint, Prog. Org. Coat. 180 (2023) 107577.
[45] Y. Liu, Z. Yu, Y. Zhang, H. Wang, Microbial dyeing for inoculation and pigment used in wood processing: opportunities and challenges, Dyes Pigments 186 (2021) 109021.
[46] S.M. Vega Gutierrez, D.W. Stone, R. He, P.T. Vega Gutierrez, Z.M. Walsh, S. C. Robinson, Potential use of the pigments from Scytalidium cuboideum and Chlorociboria aeruginosa to prevent 'Greying' decking and other outdoor wood products, Coatings 11 (2021) 511.
[47] M. Calovi, S. Rossi, Eco-friendly multilayer coating harnessing the functional features of curcuma-based pigment and rice bran wax as a hydrophobic filler, Materials 16 (2023) 7086.
[48] M. Calovi, S. Rossi, Comparative analysis of the advantages and disadvantages of utilizing spirulina-derived pigment as a bio-based colorant for wood impregnator, Coatings 13 (2023) 1154.
[49] M. Calovi, S. Rossi, Synergistic contribution of bio-based additives in wood paint: the combined effect of pigment deriving from spirulina and multifunctional filler based on carnauba wax, Prog. Org. Coat. 182 (2023) 107713.
[50] K. Prathiksha, S.J.E. Priyadharshini, J. Jacob, A.V. Jayakumar, P.H. Rao, Microalgal pigments as natural hues in environmentally-sustainable and commercially-prospective biopaints, J. Appl. Phycol. (2023) 1–14.
[51] M. Bahrami, J. Abenojar, M.A. Martínez, Comparative characterization of hot-pressed polyamide 11 and 12: mechanical, thermal and durability properties, Polymers 13 (2021) 3553.
[52] J.J. Rajesh, J. Bijwe, U. Tewari, Abrasive wear performance of various polyamides, Wear 252 (2002) 769–776.
[53] J. Bello, R. Wood, Micro-abrasion of filled and unfilled polyamide 11 coatings, Wear 258 (2005) 294–302.
[54] J.J. Balatinecz, D.E. Kretschmann, A. Leclercq, Achievements in the utilization of poplar wood–guideposts for the future, For. Chron. 77 (2001) 265–269.
[55] J.J. Balatinecz, D.E. Kretschmann, Properties and utilization of poplar wood, Poplar Culture in North America (2001) 277–291.
[56] ASTM D523-14, Standard Test Method for Specular Gloss, West Conshohocken (PA), ASTM International, 2014, pp. 1–12.
[57] ISO 2815-2000, Determinazione della durezza con il metodo di penetrazione Buchholz, UNI - Ente Nazionale Italiano di Unificazione, 2000, pp. 1–10.
[58] M. Calovi, S. Rossi, Olive pit powder as multifunctional pigment for waterborne paint: influence of the bio-based filler on the aesthetics, durability and mechanical features of the polymer matrix, Ind. Crop. Prod. 194 (2023) 116326.
[59] M. Federici, S. Gialanella, M. Leonardi, G. Perricone, G. Straffelini, A preliminary investigation on the use of the pin-on-disc test to simulate off-brake friction and wear characteristics of friction materials, Wear 410 (2018) 202–209.
[60] ASTM D4060, Standard Test Method for Abrasion Resistance of Organic Coatings by the Taber Abraser, West Conshohocken (PA), ASTM International, 2010, pp. 1–13.
[61] ISO 11998-06, Paints and Varnishes: Determination of Wet-Scrub Resistance and Cleanability of Coatings, BSI British Standards: London, UK, 2006, pp. 1–11.

[62] GB/T1733-93, Determination of Resistance to Water of Films, Standardization Administration of the People's Republic of China: Beijing, 1993, pp. 1–11.
[63] EN927-05, Paints and varnishes - coating materials and coating systems for exterior wood - part 5: assessment of the liquid water permeability, European Standard (2005) 1–18.
[64] ASTM D7334–08, Standard Practice for Surface Wettability of Coatings, Substrates and Pigments by Advancing Contact Angle Measurement, West Conshohocken (PA): ASTM International, 2008, pp. 1–3.
[65] ASTM G155-05, Operating Xenon Arc Light Apparatus for Exposure of Non-Metallic Materials, West Conshohocken, ASTM International, PA, 2005, pp. 1–11.
[66] L. Verbelen, S. Dadbakhsh, M. Van den Eynde, J.-P. Kruth, B. Goderis, P. Van Puyvelde, Characterization of polyamide powders for determination of laser sintering processability, Eur. Polym. J. 75 (2016) 163–174.
[67] H. Oliver-Ortega, J.A. Méndez, P. Mutjé, Q. Tarrés, F.X. Espinach, M. Ardanuy, Evaluation of thermal and thermomechanical behaviour of bio-based polyamide 11 based composites reinforced with lignocellulosic fibres, Polymers 9 (2017) 522.
[68] M.J. Oliveira, G. Botelho, Degradation of polyamide 11 in rotational moulding, Polym. Degrad. Stab. 93 (2008) 139–146.
[69] W.S. Tey, C. Cai, K. Zhou, A comprehensive investigation on 3D printing of polyamide 11 and thermoplastic polyurethane via multi jet fusion, Polymers 13 (2021) 2139.
[70] ASTM-E308-18, Standard Practice for Computing the Colors of Objectives by Using the CIE System, West Conshohocken, ASTM International, PA, 2018, pp. 1–45.
[71] W. Mokrzycki, M. Tatol, Colour differenceΔ E-A survey, Machine Graphics and Vision 20 (2011) 383–411.
[72] I. Calvez, S. Davoudi, C.R. Szczepanski, V. Landry, Low-gloss UV-curable coatings: light mechanisms, formulations and processes—a review, Prog. Org. Coat. 171 (2022) 107039.
[73] E. Rabinowicz, R. Tanner, Friction and wear of materials, J. Appl. Mech. 33 (1966) 479.
[74] I. Hutchings, P. Shipway, Tribology: Friction and Wear of Engineering Materials, Butterworth-Heinemann, 2017.
[75] G. Straffelini, A simplified approach to the adhesive theory of friction, Wear 249 (2001) 78–84.
[76] A. Kaboorani, N. Auclair, B. Riedl, V. Landry, Mechanical properties of UV-cured cellulose nanocrystal (CNC) nanocomposite coating for wood furniture, Prog. Org. Coat. 104 (2017) 91–96.
[77] M. Calovi, F. Russo, S. Rossi, Esthetic performance of thermochromic pigments in cataphoretic and sprayed coatings for outdoor applications, J. Appl. Polym. Sci. 138 (2021) 50622.
[78] M. Calovi, S. Rossi, F. Deflorian, S. Dirè, R. Ceccato, X. Guo, G.S. Frankel, Effects of graphene-based fillers on cathodic delamination and abrasion resistance of cataphoretic organic coatings, Coatings 10 (2020) 602.
[79] M. Calovi, F. Russo, S. Rossi, Synergic behavior of graphene-based filler and thermochromic pigments in cataphoretic coatings, Prog. Org. Coat. 150 (2021) 105978.
[80] M. Calovi, S. Rossi, Durability and thermal behavior of functional paints formulated with recycled-glass hollow microspheres of different size, Materials 16 (2023) 2678.
[81] F. Sbardella, L. Pronti, M.L. Santarelli, J.M. Asua Gonzàlez, M.P. Bracciale, Waterborne acrylate-based hybrid coatings with enhanced resistance properties on stone surfaces, Coatings 8 (2018) 283.
[82] M. Calovi, S. Rossi, The impact of stainless steel flakes as a novel multifunctional pigment for wood coatings, Journal of Coatings Technology and Research (2024) 1–17.
[83] P. Sahu, P. Mahanwar, V. Bambole, Effect of hollow glass microspheres and cenospheres on insulation properties of coatings, Pigm. Resin Technol. 42 (2013) 223–230.
[84] GB/T11186.3-90, Method of Measurement of Coating Color. Part III: Calculation of Chromatic Aberration, Standardization Administration of the People's Republic of China: Beijing, 1990, pp. 1–12.
[85] N. Huang, X. Yan, W. Zhao, Influence of photochromic microcapsules on properties of waterborne coating on wood and metal substrates, Coatings 12 (2022) 1750.
[86] M. Kluge, S. Veigel, S. Pinkl, U. Henniges, C. Zollfrank, A. Rössler, W. Gindl-Altmutter, Nanocellulosic fillers for waterborne wood coatings: reinforcement effect on free-standing coating films, Wood Sci. Technol. 51 (2017) 601–613.
[87] M. Calovi, S. Rossi, Functional olive pit powders: the role of the bio-based filler in reducing the water uptake phenomena of the waterborne paint, Coatings 13 (2023) 442.
[88] Y. Jin, Z. Su, Effects of polymerization conditions on hydrophilic groups in aromatic polyamide thin films, J. Membr. Sci. 330 (2009) 175–179.
[89] K.-Y. Law, Definitions for hydrophilicity, hydrophobicity, and superhydrophobicity: getting the basics right, in, ACS Publications (2014) 686–688.
[90] O. Chiantore, L. Trossarelli, M. Lazzari, Photooxidative degradation of acrylic and methacrylic polymers, Polymer 41 (2000) 1657–1668.
[91] H. Kaczmarek, A. Kamińska, A. van Herk, Photooxidative degradation of poly(alkyl methacrylate)s, Eur. Polym. J. 36 (2000) 767–777.
[92] M. Calovi, V. Coroneo, S. Palanti, S. Rossi, Colloidal silver as innovative multifunctional pigment: the effect of Ag concentration on the durability and biocidal activity of wood paints, Prog. Org. Coat. 175 (2023) 107354.
[93] B. Forsthuber, U. Müller, A. Teischinger, G. Grüll, Chemical and mechanical changes during photooxidation of an acrylic clear wood coat and its prevention using UV absorber and micronized TiO2, Polym. Degrad. Stab. 98 (2013) 1329–1338.
[94] M. Vlad-Cristea, B. Riedl, P. Blanchet, E. Jimenez-Pique, Nanocharacterization techniques for investigating the durability of wood coatings, Eur. Polym. J. 48 (2012) 441–453.